PLOS PATHOGENS

RESEARCH ARTICLE

MAVS mediates a protective immune response in the brain to Rift Valley fever virus

Nicholas R. Hum[1], Feliza A. Bourguet[1], Aimy Sebastian[1], Doris Lam[1], Ashlee M. Phillips[1], Kristina R. Sanchez[1¤a], Amy Rasley[1], Gabriela G. Loots[1,2], Dina R. Weilhammer[1]*

1 Biosciences and Biotechnology Division, Lawrence Livermore National Laboratory, Livermore, California, United States of America, **2** School of Natural Sciences, University of California Merced, Merced, California, United States of America

¤a Current address: Immunology Graduate Group, University of California, Davis, Davis, California, United States of America
* weilhammer1@llnl.gov

Abstract

Rift Valley fever virus (RVFV) is a highly pathogenic mosquito-borne virus capable of causing hepatitis, encephalitis, blindness, hemorrhagic syndrome, and death in humans and livestock. Upon aerosol infection with RVFV, the brain is a major site of viral replication and tissue damage, yet pathogenesis in this organ has been understudied. Here, we investigated the immune response in the brain of RVFV infected mice. In response to infection, microglia initiated robust transcriptional upregulation of antiviral immune genes, as well as increased levels of activation markers and cytokine secretion that is dependent on mitochondrial antiviral-signaling protein (MAVS) and independent of toll-like receptors 3 and 7. *In vivo*, *Mavs*$^{-/-}$ mice displayed enhanced susceptibility to RVFV as determined by increased brain viral burden and higher mortality. Single-cell RNA sequence analysis identified defects in type I interferon and interferon responsive gene expression within microglia in *Mavs*$^{-/-}$ mice, as well as dysregulated lymphocyte infiltration. The results of this study provide a crucial step towards understanding the precise molecular mechanisms by which RVFV infection is controlled in the brain and will help inform the development of vaccines and antiviral therapies that are effective in preventing encephalitis.

Author summary

Rift Valley fever virus causes severe disease in humans and livestock and in some cases can be fatal. There is concern about the use of Rift Valley fever virus as a bioweapon since it can be transmitted through the air, and there are no vaccines or antiviral treatments. Airborne transmission of the virus causes severe inflammation of the brain, yet little is known about the immune response against the virus in this organ. Here, we investigated the immune response in the brain to Rift Valley fever virus following intranasal infection. We determined that microglia, the resident immune cells of the brain, initiate a robust response to Rift Valley fever virus infection and identified a key immune pathway that is critical for the ability of microglia to respond to infection. When this immune pathway is

OPEN ACCESS

Citation: Hum NR, Bourguet FA, Sebastian A, Lam D, Phillips AM, Sanchez KR, et al. (2022) MAVS mediates a protective immune response in the brain to Rift Valley fever virus. PLoS Pathog 18(5): e1010231. https://doi.org/10.1371/journal.ppat.1010231

Editor: Amy L. Hartman, University of Pittsburgh, UNITED STATES

Received: December 23, 2021

Accepted: April 25, 2022

Published: May 18, 2022

Copyright: © 2022 Hum et al. This is an open access article distributed under the terms of the Creative Commons Attribution License, which permits unrestricted use, distribution, and reproduction in any medium, provided the original author and source are credited.

Data Availability Statement: All files for single-cell level gene expression profiles are available from the National Center for Biotechnology Information Gene Expression Omnibus accession number GSE200881.

Funding: Funding for this research was provided by internal Lawrence Livermore National Laboratory Directed Research and Development funds (17-LW-038 and 22-ERD-038 to D.W.). website: llnl.gov The funders had no role in study design, data collection and analysis, decision to publish, or preparation of the manuscript.

Competing interests: The authors have declared that no competing interests exist.

rendered non-functional, mice have a dysregulated response to infection in the brain. This study provides insight into how the immune response can control Rift Valley fever virus infection of the brain.

Introduction

Rift Valley fever virus (RVFV) (genus *Phlebovirus*/family *Phenuviridae*), is a highly pathogenic mosquito-borne virus that can cause lethal disease in both humans and livestock, including acute-onset hepatitis, delayed-onset encephalitis, blindness, or hemorrhagic fever [1]. RVFV is endemic to Africa however concern exists about its potential spread across the world, similar to Zika or West Nile virus (WNV) [1]. Outside of Africa, competent vectors for RVFV include over 30 species of mosquitoes that are present throughout North and South America [2]. RVFV is also classified as a Category A Biodefense pathogen by the National Institute of Allergy and Infectious Diseases (NIAID) due to the potential for intentional spread by aerosol and the lack of licensed vaccines or antiviral therapeutics. Furthermore, RVFV is classified by the Department of Health and Human Services (HHS) and United States Department of Agriculture (USDA) as an overlap select agent due to the susceptibility of numerous livestock species to this disease [3].

In the event of an intentional release, the most likely route of exposure to RVFV would be through the respiratory system via aerosolized release of the virus. Studies conducted using rodent models indicate a more severe infection following respiratory versus subcutaneous exposure, with higher incidence of lethality, neuropathology, and increased viral titers in the brain [4–7]. Analysis of human infections also suggests that aerosol exposure to RVFV (i.e., laboratory acquired infections and infections acquired via handling of infected livestock) leads to a higher incidence of severe disease with encephalitis and long-lasting neurologic complications [8,9]. The fatality rate amongst patients with encephalitic manifestations of disease is ~50% [10], which is much higher than the overall fatality rate, estimated to be between 0.5–2% [11]. Thus, a thorough understanding of RVFV pathogenesis in the brain is required for preparedness to combat the virus' worst outcomes, including intentional release of the virus.

The term "immune privileged site" was once applied to the brain and interpreted to mean that few immune defenses were functional in this organ [12]. However, it is now widely accepted that the brain is highly immunologically active [13]. An emerging body of evidence indicates that immune responses within the brain are critical for control of an array of neuroinvasive viruses [14,15]. In the brain, neurons, and glial cells (e.g., astrocytes, and microglia), express many of the same pattern recognition receptors (PRRs) expressed by cells in the periphery and initiate type I interferon (IFN) expression as well as other innate responses upon viral infection [15,16]. Such early responses in the brain are critical for direct control of viral replication, as well as for recruitment of adaptive immune cells that participate in viral clearance [17,18]. Microglia, the resident immune cells of the brain, play a key role in bridging innate and adaptive immune responses in the brain [19–21], and depletion of microglia increases susceptibility to multiple viral infections [18,22,23]. Although potent immune responses are required for viral control in the brain, limiting inflammation presents a unique immunoregulatory challenge as excessive inflammation can be especially deleterious and promote neurodegenerative diseases such as Parkinson's [24] and Alzheimer's [25] disease. Thus, investigation of immune responses in the brain presents an opportunity to understand the interaction of processes that hone the correct response to control viral replication without inducing excessive damaging inflammation.

To date, there has been limited investigation of the immune response to RVFV in the brain. Previous work has indicated that a strong adaptive response involving both CD4 and CD8 T cells as well as a robust antibody response is required for the prevention of encephalitic disease [7,26,27] yet there remains a lack of understanding of the response of resident and infiltrating immune cells in the brain. Furthermore, the PRRs that microglia use to respond to RVFV infection have not yet been identified. Previous work has demonstrated the critical role of RIG-I-like receptor (RLR) signaling *via* mitochondrial antiviral signaling (MAVS) in the type I IFN response of macrophages and dendritic cells (DCs) to RVFV infection, as well as a protective role for MAVS following *in vivo* challenge, with little to no contribution from the RNA-sensing toll-like receptors (TLRs) [6]. However, differential roles for the RNA-sensing PRRs during viral infections of the CNS have been identified, most notably for West Nile Virus (WNV), where TLR3, TLR7, and RLR receptors RIG-I and MDA-5 have been shown to coordinate and propagate a protective response [28–30]. Identifying the relative contributions of innate signaling pathways to the induction of type I IFNs and subsequent control of viral infection has important consequences in terms of understanding human susceptibility to RVFV infection, as polymorphisms in TLR3, TLR7, their respective downstream signaling adaptors TRIF and MyD88, as well as RIG-I and MAVS have all been associated with severe disease/neuropathology in humans [31].

Here, we investigated the immune response in the murine brain to RVFV intranasal infection. We demonstrate that microglia mount a robust response that is dependent on MAVS and independent of TLR3 and TLR7. MAVS is critical for the expression of immunoregulatory genes, secretion of cytokines, and upregulation of surface markers of activation. *Mavs*$^{-/-}$ mice are more susceptible to infection, with higher viral titers in the brain following intranasal challenge. RNA sequence (RNA-seq) analysis of whole brain tissue revealed robust immune gene expression with greater induction of inflammatory genes in the brains of *Mavs*$^{-/-}$ versus wild type (WT) mice. Single cell RNA-sequence (scRNA-seq) analysis revealed defects in specific antiviral genes and signaling pathways within microglia in the brains of RVFV infected *Mavs*$^{-/-}$ mice. The lack of MAVS resulted in a shift towards a more inflammatory phenotype, with a decrease in antiviral signaling pathways and an increase in proinflammatory pathways within *Mavs*$^{-/-}$ microglia. Differences in immune infiltration into the brain were also observed between WT and *Mavs*$^{-/-}$ mice. These results are an important step towards understanding the cell types and molecular pathways responsible for controlling RVFV infection in the brain and towards future developments of antiviral treatments.

Results

RVFV infection induces a robust response in microglia that is dependent upon MAVS and independent of TLR3 and TLR7

To determine if microglia respond to RVFV infection directly *via* cell intrinsic mechanisms, we first confirmed infection of microglia cell lines EOC 13.31 and SIM A9, as well as primary microglia derived from the brains of neonatal mice *via* flow cytometry using a RVFV-specific antibody (Fig 1A and 1B). Vero cells were also included as a positive control for infection. EOC 13.31 cells had the lowest infectivity rate ranging from 30–40% positive cells, while primary microglia displayed infectivity rates (50–70%) similar to SIM A9 cells (60–70%) but slightly less than the Vero positive control (90%) (Fig 1B). Both the fully virulent (ZH501) and attenuated (MP-12) strains of RVFV yielded similar levels of infected primary microglia (Fig 1C). Next, we probed the response of primary microglia to both the MP-12 and ZH501 strains by quantifying changes in expression of genes involved in antiviral immune responses using real-time reverse transcription (RT^{2}) PCR array (Fig 1D and 1E and S1 Table). There was a

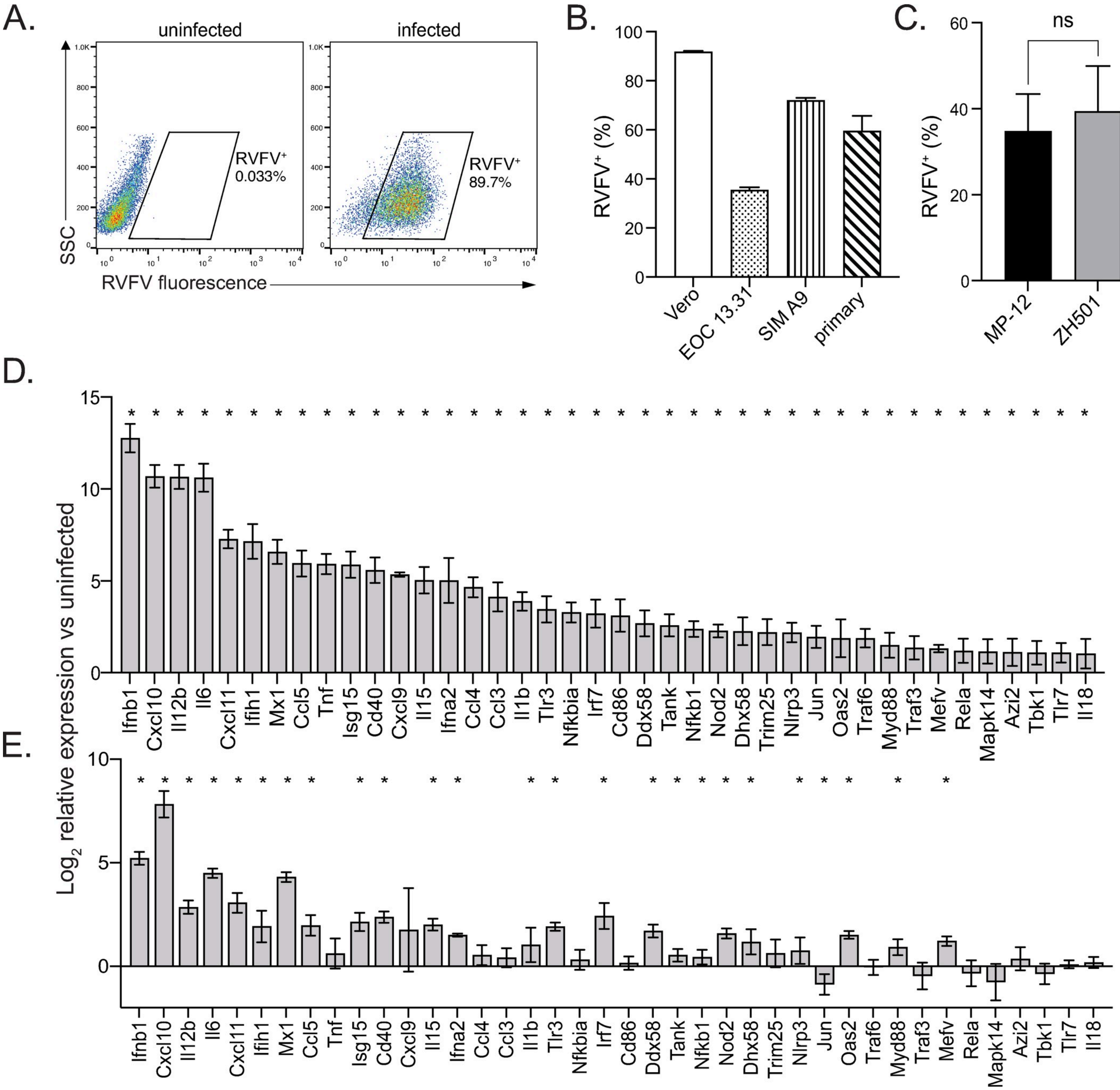

Fig 1. RVFV infects microglia. Microglia cell lines EOC 13.31 and SIM A9 and primary microglia derived from the brains of neonatal mice, along with Vero positive control cells, were infected with RVFV MP-12. The percentage of cells positive for RVFV was assessed by flow cytometry. Representative plots of Vero cell infection analysis (A). RVFV infection rate for all cell types (B). Primary microglia derived from wildtype (WT) mice were infected with RVFV MP-12 or ZH501 and the percentage of cells positive for RVFV was assessed by flow cytometry (C). The relative expression of 40 antiviral response genes with the highest fold change in infected versus uninfected cells (D). Data in (B-C) are shown as the mean +/- SD. Data in (D) and (E) are shown as the mean log$_2$ fold change in infected versus uninfected cells +/- SEM. *denotes significant changes in gene expression beyond 95% CI between uninfected vs infected cells.

https://doi.org/10.1371/journal.ppat.1010231.g001

significant response to both viruses with similar patterns of gene expression changes, although the overall magnitude of the response was greater in microglia infected with the attenuated versus the fully virulent strain, consistent with prior reports [32]. 40 significantly upregulated antiviral response genes were observed upon MP-12 microglial infection, whereas 25 of these genes were significantly upregulated in ZH501 infected microglia. The response to MP-12 was robust, with very high levels of *Ifnb1* expression (greater than 6,000-fold upregulation) and greater than 10-fold upregulation of over 20 genes, including *Ifna2*, *Ifih1*, *Isg15*, *Cxcl10*, *Il6*, and *Il12b*, among others. Notably, significant *Ifnb1* and *Ifna2* induction was observed in ZH501 infected microglia, albeit to lower levels than MP-12 infected microglia.

Next, microglia derived from WT, *Tlr3*$^{-/-}$, *Tlr7*$^{-/-}$, or *Mavs*$^{-/-}$ mice were infected with MP-12, and a similar infectivity rate was confirmed amongst all groups, therefore was independent of genotype (S1A Fig). Microglia derived from TLR3 or TLR7 deficient animals activated immune genes in response to RVFV at levels similar to WT microglia (Fig 2A and 2B and S1 Table). Out of the 40 most differentially expressed genes, only 2 displayed significant differences in expression between WT and *Tlr3*$^{-/-}$, and 9 genes had significant differences in expression between WT and *Tlr7*$^{-/-}$. In contrast, microglia derived from *Mavs*$^{-/-}$ mice displayed an abrogated response to infection, with minimal changes in gene expression in most genes in the array and a greater than 4,000-fold reduction in *Ifnb1* expression versus WT infected microglia (Fig 2C and S1 Table). 31 of the 40 top differentially expressed genes displayed significant differences in expression between WT and *Mavs*$^{-/-}$. To confirm that differences in gene expression observed between WT and *Mavs*$^{-/-}$ microglia were not due to differences in the level of infection, RVFV genomic RNA was quantified, and comparable levels were detected in microglia of both genotypes (S1B Fig). Comparable growth of the virus within microglia of both genotypes was further confirmed by the quantification of viral titer within supernatants collected from WT and *Mavs*$^{-/-}$ microglia (S1C Fig).

We further characterized the role of MAVS in the response of microglia to RVFV infection *in vitro* by assessing expression of microglial activation markers as well as cytokine secretion (Fig 3). Microglia upregulated surface expression of CD86, CD80, and I-A/I-E in a MAVS-dependent manner (Fig 3A). Using RVFV antibody staining, cells within infected cultures could be identified as infected (RVFV^{+}) or uninfected (RVFV^{-}). Expression was upregulated not only on infected microglia (RVFV^{+}), but also on uninfected cells within the culture (RVFV^{-}), suggesting secreted cytokines can influence the activation state of cells in trans. Within WT microglia, expression of each marker was highest on infected cells, with an intermediate level of expression seen on cells activated in trans. On *Mavs*$^{-/-}$ microglia, apart from a low level of CD80 on infected cells, no significant upregulation of activation markers was observed. In contrast, upregulation of activation markers was unaltered from WT on *Tlr3*$^{-/-}$ and *Tlr7*$^{-/-}$ microglia (S2 Fig).

Cytokine secretion by infected microglia was also dependent on MAVS (Fig 3B). High levels of type I IFNs were detected in supernatants from WT infected cells, as well the inflammatory cytokines IL-6 and TNF-α, and chemokines CCL5, CXCL10, CXCL11, and CCL2. Cytokine levels in supernatants from MAVS-deficient cells were not detectable or not significantly different from uninfected supernatants. Taken together, these data demonstrate that microglia have a robust response to RVFV infection that is mediated primarily through the RLR signaling adaptor MAVS.

Mavs$^{-/-}$ animals have a dysregulated immune response with increased susceptibility to infection

We then investigated the role of MAVS in the immune response in the brain during *in vivo* challenge with RVFV (Fig 4). Intranasal challenge of WT and *Mavs*$^{-/-}$ cohorts of mice ($n = 20$) with the ZH501 strain of RVFV confirmed enhanced susceptibility to infection of *Mavs*$^{-/-}$ mice, consistent with prior reports [6]. *Mavs*$^{-/-}$ mice succumbed to challenge significantly faster, with 100% of *Mavs*$^{-/-}$ mice deceased by 6 days post-infection, whereas 20% of WT animals were still alive 10 days post-infection (Fig 4A).

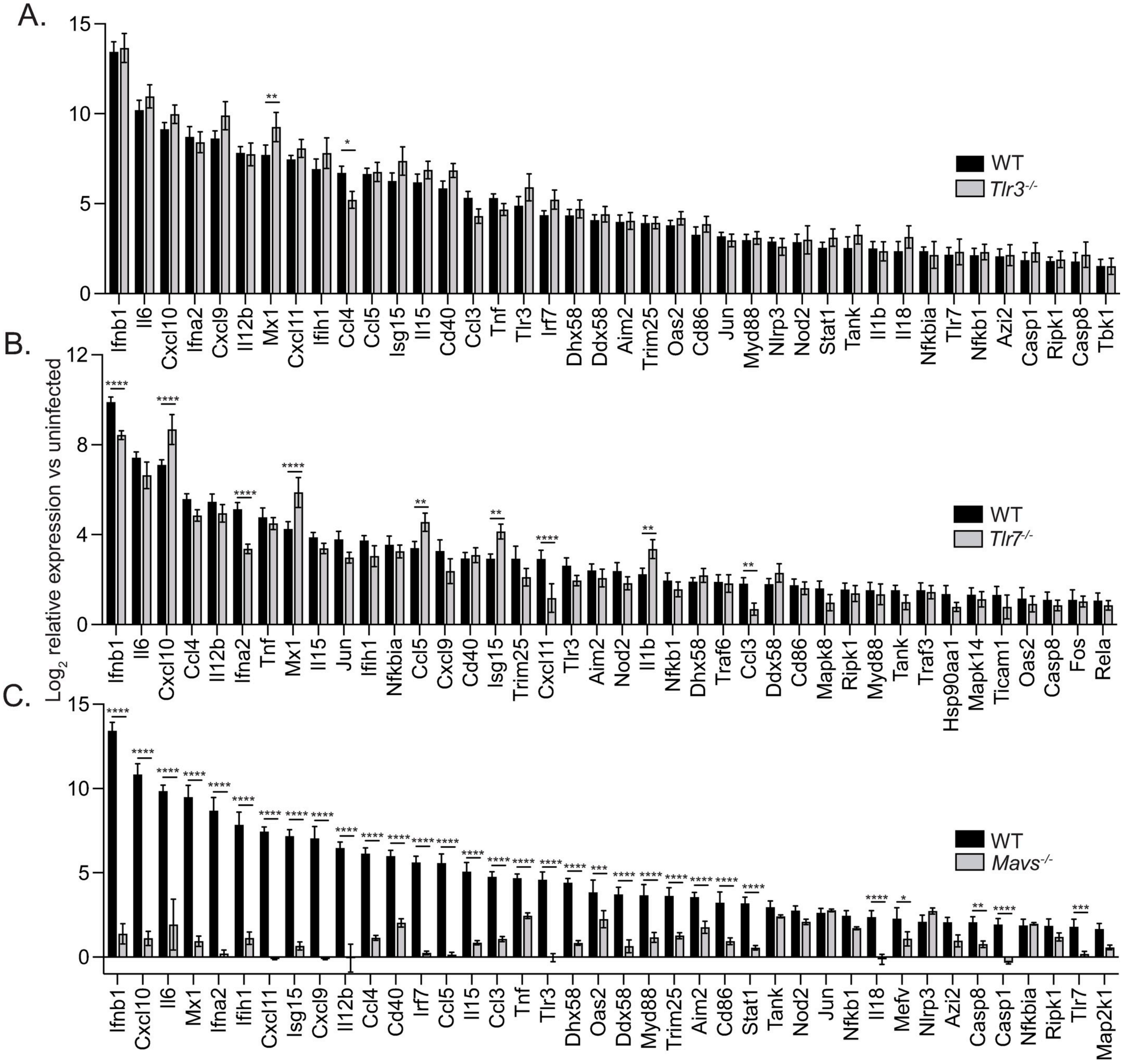

Fig 2. Microglial response to RVFV infection is dependent upon MAVS and independent of TLR7 and TLR3. Primary microglia derived from WT or *Tlr3*$^{-/-}$ (A), *Tlr7*$^{-/-}$ (B) or *Mavs*$^{-/-}$ (C) mice were infected with RVFV MP-12. The relative expression of 40 antiviral response genes with the highest fold change in WT cells are shown as the mean log$_2$ fold change in infected versus uninfected cells, +/- SD. *p <0.05, **p<0.01, ***p<0.001, ****p<0.0001.

https://doi.org/10.1371/journal.ppat.1010231.g002

To facilitate the assessment of antiviral responses by multiple cellular and molecular modalities, we utilized the MP-12 strain for further analysis, which can be handled at biosafety level 2 containment. Previous work has utilized the MP-12 strain in a C57BL/6 mouse model of intranasal infection to investigate RVFV pathogenesis and found that while WT mice did not have detectable viremia over the course of the evaluation period (0–8 days post-infection), 50% of animals succumbed to lethal infection between days 8–14 post-infection [6]. Therefore, WT animals are susceptible to infection and thus should be expected to have measurable immune

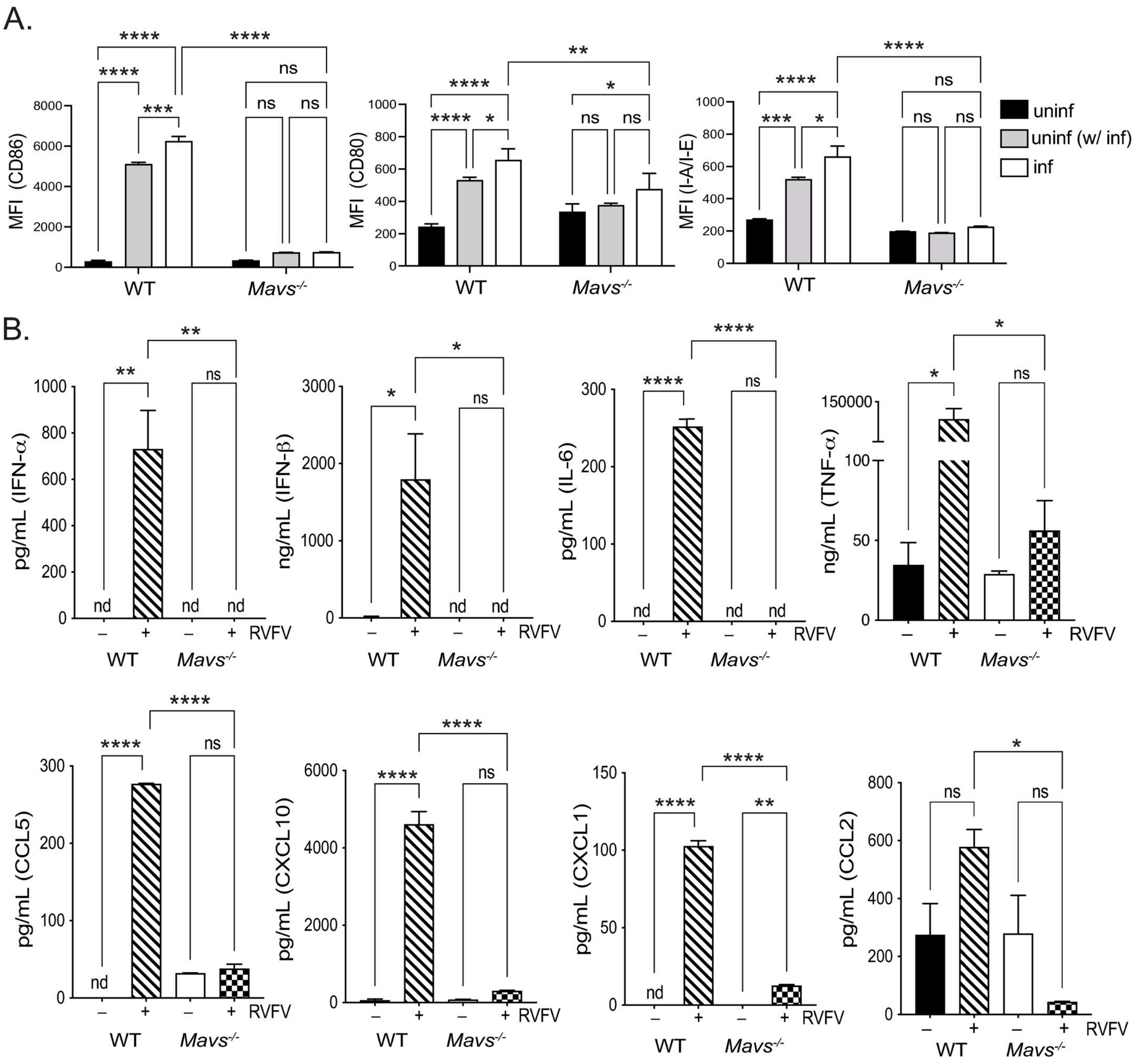

Fig 3. Microglia respond to RVFV infection in vitro by cytokine secretion and upregulation of activation markers. Microglia derived from WT or *Mavs*$^{-/-}$ mice were infected with RVFV MP-12 and at 18–24 h post-infection, cells and cellular supernatants were harvested for flow cytometry and multiplex cytokine analysis, respectively. The expression levels of the indicated activation markers were assessed on uninfected cells (black bars), uninfected cells in culture with infected cells (uninf (w/ inf), gray bars), and infected cells (inf, white bars) and shown as the mean fluorescence intensity of the indicated activation markers (A). Cytokine levels in cellular supernatants (B). Data are shown as the mean +/- SD, nd = not detected and was denoted as zero $^{*}p < 0.05$, $^{**}p < 0.01$, $^{***}p < 0.001$, $^{****}p < 0.0001$.

https://doi.org/10.1371/journal.ppat.1010231.g003

responses. Viral titers in the brain were not assessed as part of this study, therefore we conducted a longitudinal study over 4 days where brains of infected WT mice were examined *ex vivo* to identify live virus derived from brain tissue following intranasal challenge (S3 Fig). Day 7 post-infection was the earliest timepoint live virus could be detected in infected WT brains, thus day 7 was selected as the time point for all further analyses, as we were interested in capturing early innate antiviral responses.

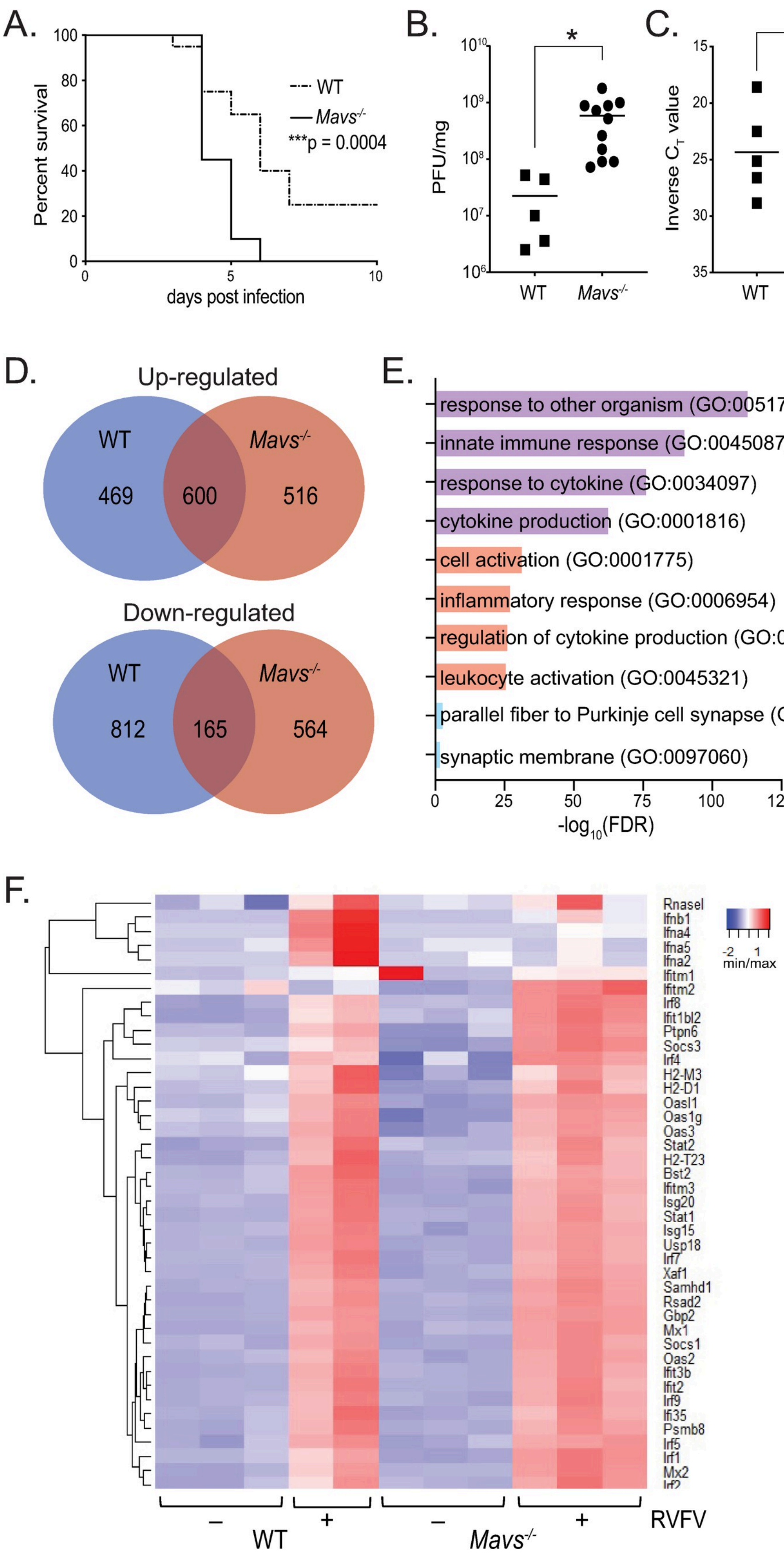
A.
Percent survival
100
80
60
40
20
0
days post infection
0
5
10
WT
Mavs-/-
***p = 0.0004
B.
PFU/mg
10^{10}
10^9
10^8
10^7
10^6
*
WT
Mavs-/-
C.
Inverse C_T value
15
20
25
30
35
*
WT
Mavs-/-
D.
Up-regulated
WT
Mavs-/-
469
600
516
Down-regulated
WT
Mavs-/-
812
165
564
E.
response to other organism (GO:0051707)
innate immune response (GO:0045087)
response to cytokine (GO:0034097)
cytokine production (GO:0001816)
cell activation (GO:0001775)
inflammatory response (GO:0006954)
regulation of cytokine production (GO:0001817)
leukocyte activation (GO:0045321)
parallel fiber to Purkinje cell synapse (GO:0098688)
synaptic membrane (GO:0097060)
0
25
50
75
100
125
$-\log_{10}(FDR)$
F.
Rnasel
Ifnb1
Ifna4
Ifna5
Ifna2
Ifitm1
Ifitm2
Irf8
Ifit1bl2
Ptpn6
Socs3
Irf4
H2-M3
H2-D1
Oasl1
Oas1g
Oas3
Stat2
H2-T23
Bst2
Ifitm3
Isg20
Stat1
Isg15
Usp18
Irf7
Xaf1
Samhd1
Rsad2
Gbp2
Mx1
Socs1
Oas2
Ifit3b
Ifit2
Irf9
Ifi35
Psmb8
Irf5
Irf1
Mx2
Irf2
-2
1
min/max
–
+
–
+
RVFV
WT
Mavs-/-

Fig 4. *Mavs*$^{-/-}$ mice are more susceptible to intranasal RVFV infection and display increased viral burden and immune gene expression in the brain. WT or *Mavs*$^{-/-}$ mice were infected intranasally with 1000 PFU RVFV ZH501 (A), or 5x10^{5} PFU RVFV MP-12 (B-E). Morbidity and mortality were assessed daily, and percent survival is depicted in (A). On day 7 post-infection (B-E), brains were processed for viral quantitation and RNA extraction. Viral quantitation by PFU (B) and genomic RNA (C). Genes differentially expressed between uninfected and infected brains (D). Functional enrichment of differentially expressed genes (E). Ontologies that were enriched in both WT and *Mavs*$^{-/-}$ infected brains are highlighted in purple. Pathways enriched only in *Mavs*$^{-/-}$ or WT infected brains are highlighted in red and blue, respectively. Heatmap of IFN α/β signaling genes (F). $^{*}p<0.05$, $^{***}p<0.001$.

https://doi.org/10.1371/journal.ppat.1010231.g004

Next, we compared disease progression between WT and *Mavs*$^{-/-}$ mice. Little to no clinical signs of infection were observed in WT mice by day 7, with 11 of 12 mice displaying normal behavior and healthy appearance. One WT mouse displayed neurological signs of disease (cage circling). *Mavs*$^{-/-}$ mice, in contrast, uniformly displayed signs of illness with decreased signs of activity and 4 of 12 mice displaying neurological signs of disease (head tilt or cage circling). One *Mavs*$^{-/-}$ mouse required euthanizing on day 6 due to moribund appearance. We next assessed viral titers in the brain and were able to detect live virus in 100% of *Mavs*$^{-/-}$ (n = 11), but only in 42% of WT (n = 12) infected brains. Within brains with detectable virus, titers (Fig 4B) as well as the levels of RVFV genomic RNA (Fig 4C) were significantly higher in *Mavs*$^{-/-}$ than in WT mice.

To assess the antiviral response, we utilized RNA-seq to profile the transcriptomic alterations induced by RVFV infection in the brains of WT and *Mavs*$^{-/-}$ mice. Infection resulted in significant upregulation of 1,069 genes in the brains of WT mice and 1,116 genes in the brains of *Mavs*$^{-/-}$ mice where 600 upregulated genes were in common to both WT and *Mavs*$^{-/-}$ (Fig 4D and S2 Table). Downregulation of genes in response to infection displayed less overlap between WT and *Mavs*$^{-/-}$, with 977 downregulated in WT, 729 downregulated in *Mavs*$^{-/-}$, and only 165 downregulated genes common to both genotypes (Fig 4D). Functional enrichment of differentially expressed genes revealed strong correlation of pathways related to innate immune and defense responses in both WT and *Mavs*$^{-/-}$ brains, including response to other organism (GO:0051707), innate immune response (GO:0045087), response to cytokine (GO:0034097), and cytokine production (GO:0001816) (Fig 4E).

To identify deficiencies in the antiviral response within *Mavs*$^{-/-}$ brains that would indicate the effector functions downstream of MAVS signaling that control viral replication, we focused on pathways that were enriched in WT and unaffected in *Mavs*$^{-/-}$ infected brains. Interestingly, only two pathways were enriched in WT and not *Mavs*$^{-/-}$ yet neither are involved in immune responses nor indicate any functional advantage WT animals have at controlling viral replication (Fig 4E). *Mavs*$^{-/-}$ brains had more exclusively enriched pathways, including regulation of cytokine production (GO:0001817) and inflammatory response (GO:0006954), indicating that the overall levels of inflammation were higher in *Mavs*$^{-/-}$ brains than in WT. This is consistent with previous reports that indicated a more robust serum cytokine response in *Mavs*$^{-/-}$ than WT mice infected with RVFV [6].

IFN α/β gene expression levels were elevated in WT infected brains, whereas induction was not seen in *Mavs*$^{-/-}$ brains (Fig 4F). However, upregulation of genes downstream of type I interferons was observed to a similar extent in the brains of WT and *Mavs*$^{-/-}$ infected mice. Thus, while a deficiency in type I interferons is noted in *Mavs*$^{-/-}$ brains, examination of downstream signaling does not reveal potential deficiencies in antiviral response genes. In total, the data demonstrate that RVFV infection results in robust activation of immune and inflammatory genes in both WT and *Mavs*$^{-/-}$ brains with very similar patterns of gene upregulation in both.

Single cell RNA sequencing reveals changes in immune infiltration and signaling defects in microglia following RVFV infection of *Mavs*$^{-/-}$ mice

Next, we performed scRNA-seq to increase the resolution of transcriptional analysis and assess cellular variations resulting from the absence of MAVS during RVFV infection of the brain. Single cell suspensions were generated from whole brain tissue of WT and *Mavs*$^{-/-}$ mice, with (WT+, *Mavs*$^{-/-}$+) and without (WT-, *Mavs*$^{-/-}$−) RVFV infection. The following cell numbers were sequenced from a single mouse (male) for each condition: WT-: 1,989, *Mavs*$^{-/-}$−: 1,749, WT+: 1627, *Mavs*$^{-/-}$−: 1841, for a total of 7,206 cells. Unsupervised clustering of the data resulted in 12 cell type clusters (Fig 5A). By cross-referencing genes differentially expressed in each cluster to previously published cell-type specific markers [33–36], we assigned each cluster to its putative cell-type identity (S4A Fig). We identified expected cell clusters such as neurons, astrocytes, oligodendrocytes, and endothelial cells. Three clusters of immune cells were identified, corresponding to microglia/myeloid cells, T/natural killer (NK) cells, and neutrophils. We observed a large shift in the relative frequency of immune cells upon infection, indicating massive immune infiltration in the brains of infected animals (Fig 5B and 5C). Sequenced cells from uninfected brains were comprised of 70–80% non-immune cells (clusters 1, 2, 4–9, and 11), with immune cells (clusters 0, 3, and 10) comprising less than 30%. In contrast, sequenced cells from infected brains were comprised of 30–40% non-immune and more than 60% immune cells (Fig 5B and 5D). Interestingly, the pattern of immune infiltration differed between WT and *Mavs*$^{-/-}$ infected brains. WT animals exhibited infiltration of mostly myeloid lineage cells, whereas *Mavs*$^{-/-}$ animals exhibited infiltration of lymphocyte populations in addition to myeloid lineage cells (Fig 5D). This pattern of immune infiltration, with a substantial number of myeloid cells in both genotypes and a larger number of lymphocytes in *Mavs*$^{-/-}$ versus WT, was confirmed in a second set of infected brains analyzed by scRNA-seq isolated from female mice (S4B Fig).

Immune infiltration was also confirmed using flow cytometry (Fig 5E–5G) and was consistent with scRNA-seq ratios. Lymphocytes and non-glial cells of myeloid lineage comprised a very small fraction of immune cells within uninfected brains, ranging from 0.5–4% and 1–6% of brain immune cells, respectively (Fig 5F and 5G). In contrast, the percentage of non-glial myeloid cells increased to 10–25% of brain immune cells in both WT and *Mavs*$^{-/-}$ infected mice (Fig 5F). Lymphocytes also increased in the brains of both WT and *Mavs*$^{-/-}$ infected mice, however significantly more lymphocytes were observed in the brains of *Mavs*$^{-/-}$ mice (Fig 5G), with lymphocytes comprising 5–15% of brain immune cells in WT mice and 15–30% of brain immune cells in *Mavs*$^{-/-}$ mice.

Analysis of IFN α/β and downstream signaling gene expression within individual cell clusters revealed that type I IFN (*Ifnb1* and *Ifna2*) were primarily expressed by microglia/myeloid cells (cluster 0), astrocytes (cluster 1), and oligodendrocytes (cluster 7) (Fig 5D). While limited expression of IFN response genes was observed within T/NK cells (cluster 3) and endothelial cells (cluster 8), most expression was observed within microglia/myeloid cells (cluster 0). Although neutrophils (cluster 10) also expressed IFN response genes, neutrophils only constituted a small fraction of cells in infected brains (Fig 5A). Little to no gene expression was observed in neuronal cell clusters 4, 5, and 11.

Clustering of microglia/myeloid cells (cluster 0, Fig 5A) identified 6 subclusters of myeloid cells (Fig 6A). Enumeration of cells according to condition suggested that most immune cells present in uninfected brains were microglia, whereas infected brains contained cells of multiple infiltrating lineages including monocytes, antigen presenting cells (APCs), and granulocytic cells (Fig 6B and 6D). The distribution of myeloid lineage cells in uninfected brains confirmed the flow cytometry data in Fig 5E and is consistent with previously published

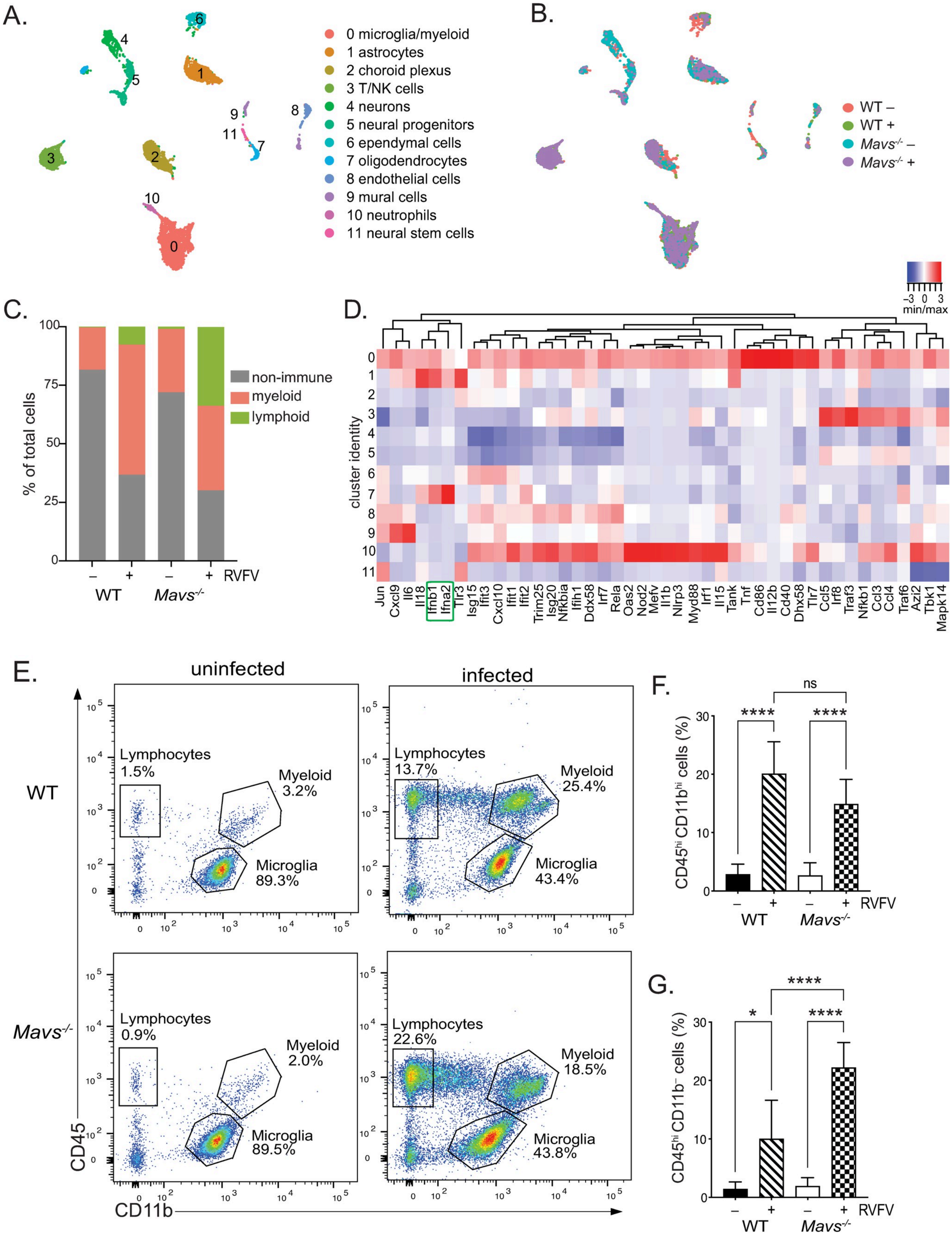
A.
0 microglia/myeloid
1 astrocytes
2 choroid plexus
3 T/NK cells
4 neurons
5 neural progenitors
6 ependymal cells
7 oligodendrocytes
8 endothelial cells
9 mural cells
10 neutrophils
11 neural stem cells
B.
WT –
WT +
Mavs-/- –
Mavs-/- +
C.
% of total cells
100
75
50
25
0
non-immune
myeloid
lymphoid
– + – + RVFV
WT Mavs-/-
D.
-3 0 3
min/max
cluster identity
0 1 2 3 4 5 6 7 8 9 10 11
Jun Cxcl9 Il6 Il18 Ifnb1 Ifna2 Tlr3 Isg15 Ifit3 Cxcl10 Ifit1 Ifit2 Trim25 Isg20 Nfkbia Ifih1 Ddx58 Irf7 Rela Oas2 Nod2 Mefv Il1b Nlrp3 Myd88 Irf1 Il15 Tank Tnf Cd86 Il12b Cd40 Dhx58 Tlr7 Ccl5 Irf8 Traf3 Nfkb1 Ccl3 Ccl4 Traf6 Azi2 Tbk1 Mapk14
E.
uninfected
infected
WT
Mavs-/-
Lymphocytes 1.5%
Myeloid 3.2%
Microglia 89.3%
Lymphocytes 13.7%
Myeloid 25.4%
Microglia 43.4%
Lymphocytes 0.9%
Myeloid 2.0%
Microglia 89.5%
Lymphocytes 22.6%
Myeloid 18.5%
Microglia 43.8%
CD45
CD11b
0 10^2 10^3 10^4 10^5
F.
CD45hi CD11bhi cells (%)
30 20 10 0
**** ns ****
– + – + RVFV
WT Mavs-/-
G.
CD45hi CD11b– cells (%)
30 20 10 0
* **** ****
– + – + RVFV
WT Mavs-/-

Fig 5. Single cell RNA sequencing reveals shifts in cell populations and immune infiltration in the brain following RVFV infection. UMAP plots depicting cell clusters derived from WT and *Mavs*$^{-/-}$ brains, +/- RVFV infection. Cell types (A) or conditions (B) are color coded. The distribution of cell types within brains of each condition (C). A heatmap of IFN α/β signaling genes across cell clusters (defined in (A)) is shown in (D). *Ifnb1* and *Ifna2* are highlighted in green. Flow cytometry: Representative plots of CD11b vs CD45 and the gates defining microglia, lymphocytes, and myeloid cells are shown for uninfected (left panels) and infected brains (right panels) isolated from WT (top panels) and *Mavs*$^{-/-}$ (bottom panels) mice (E). The percent myeloid cells (CD11b^{hi} CD45^{hi}), and lymphocytes (CD11b^{-} CD45^{hi}) (F) and (G), respectively. Data in (F) and (G) are shown as the mean +/- SD. $^{*}p<0.05$, $^{***}p<0.001$, $^{****}p<0.0001$.

https://doi.org/10.1371/journal.ppat.1010231.g005

reports [37] which indicate that microglia are the predominant immune cell type in the brain under non-pathological conditions. The relative frequency of macrophages (cluster 4) was consistent across conditions and likely corresponds to resident non-parenchymal macrophages [38], rather than an infiltrated population. Infected brains of both genotypes demonstrated similar patterns of monocyte, APC, and granulocytic cell infiltration (clusters 2, 3, and 5, respectively). Overall, the distribution of myeloid cells was similar between infected brains of both genotypes.

Next, we examined transcriptional differences in the antiviral responses of microglia derived from WT and *Mavs*$^{-/-}$ infected brains. Differences in *Ifnb1* and *Ifna2* expression were noted in a subset of microglia in WT infected brains whereas levels were undetectable in microglia from *Mavs*$^{-/-}$ infected and uninfected brains of both genotypes (Fig 6E). Similarly, expression of *Ifnb1* and *Ifna2* were also dependent upon MAVS in astrocytes and oligodendrocytes (S4C and S4D Fig, respectively). Gene ontological analysis revealed specific enrichment of pathways involved in antiviral responses including response to virus (GO:009615), negative regulation of viral genome replication (GO:0045071), antigen processing and presentation (GO:0019882), and response to type I interferon (GO:0034340) within WT infected microglia (Fig 6F). In contrast, inflammatory pathways such as response to interleukin-1 (GO:007055) and positive regulation of interleukin-6 production (GO:0032755), as well as pathways involved in cell migration such as regulation of chemokine production (GO:0032642) and positive regulation of cell adhesion (GO:0045785) were enriched in *Mavs*$^{-/-}$ microglia (Fig 6G). Specific IFN-stimulated genes (ISGs) were expressed at higher levels within WT microglia, including *Irf7*, *Isg20*, *Isg15*, *Oasl1*, *Ifit1*, *Ifit3*, *Ifi27l2a*, and *Bst2* (Fig 6H). Genes that have been previously associated with a pro-inflammatory state [39–41] were expressed at higher levels within *Mavs*$^{-/-}$ microglia, including *Irf1*, *Irf8*, *Il1b*, and *Nos2* (Fig 6H). A similar pattern of increased IFN-stimulation was also observed within WT female infected brains relative to *Mavs*$^{-/-}$ (S4E Fig).

Flow cytometric analysis revealed further defects in *Mavs*$^{-/-}$ microglia. In line with increased viral titers in the brains of *Mavs*$^{-/-}$ animals (Fig 4B), microglia from *Mavs*$^{-/-}$ animals displayed dramatically higher levels of infection as evidenced by anti-RVFV antibody staining, ranging from 0.5–9% in WT brains to 15–50% in *Mavs*$^{-/-}$ brains (Fig 6I). We also evaluated the surface expression levels of activation markers; expression of CD86 mirrored *in vitro* results, with WT microglia that are RVFV^{+} expressing the highest levels of CD86, and microglia from infected brains that are RVFV^{-} expressing an intermediate level of CD86, although not significantly different from microglia from uninfected brains (Fig 6J). There was no significant upregulation of CD86 on microglia from *Mavs*$^{-/-}$ brains. Expression of I-A/I-E was also elevated on RVFV^{+} microglia, although not on RVFV^{-} microglia, from WT infected brains (Fig 6K). In contrast to *in vitro* results, upregulation of I-A/I-E was detected on microglia derived from *Mavs*$^{-/-}$ brains (Fig 6K). No significant upregulation of CD80 was detected (S5 Fig).

Lymphocyte infiltration and signaling defects in the brains of *Mavs*$^{-/-}$ mice

The majority of lymphocytes identified within WT infected brains were NK cells, whereas those in *Mavs*$^{-/-}$ infected brains included a high abundance of T cells in addition to NK cells

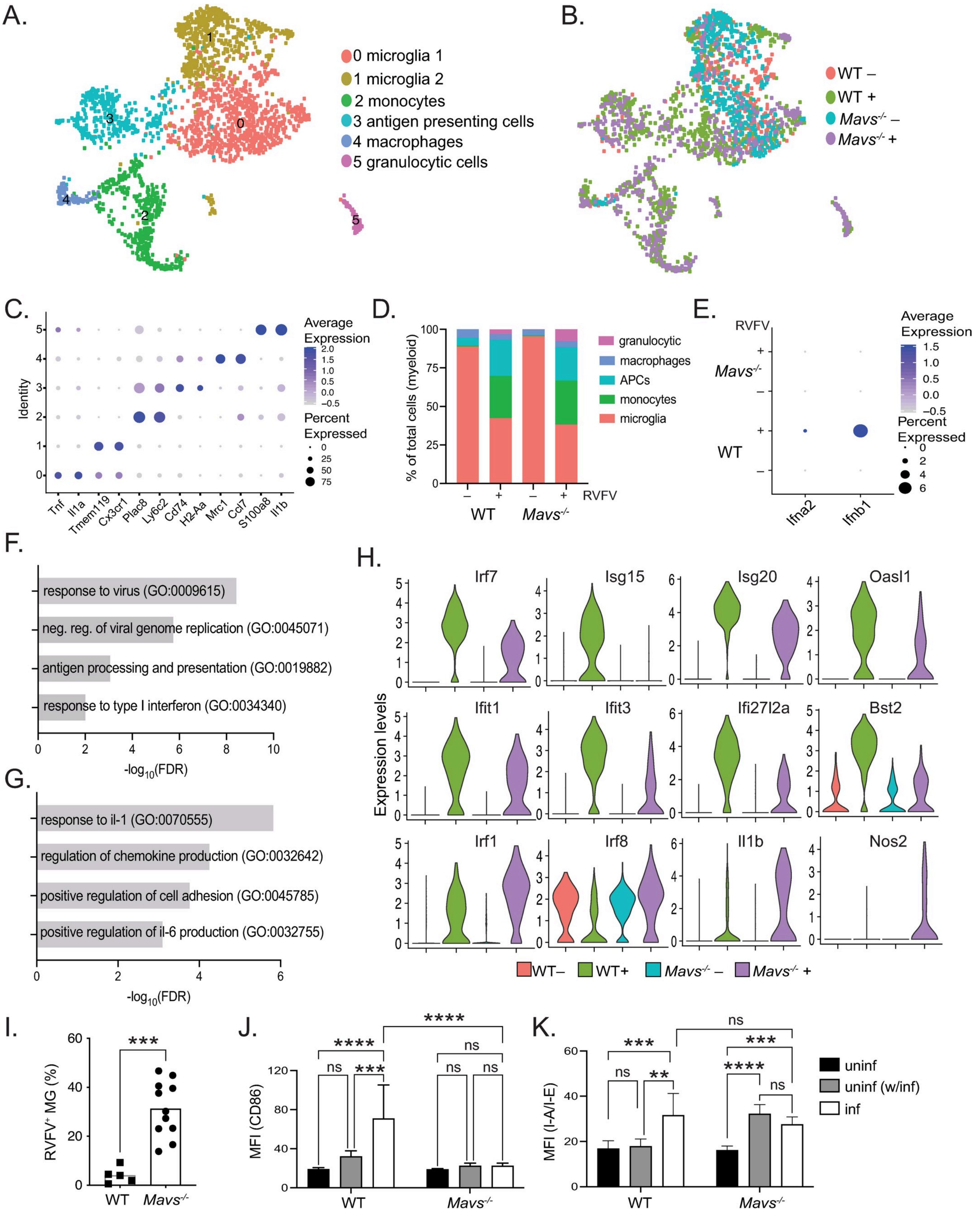
A.
0 microglia 1
1 microglia 2
2 monocytes
3 antigen presenting cells
4 macrophages
5 granulocytic cells
B.
WT –
WT +
Mavs-/- –
Mavs-/- +
C.
Identity
Tnf Il1a Tmem119 Cx3cr1 Plac8 Ly6c2 Cd74 H2-Aa Mrc1 Ccl7 S100a8 Il1b
Average Expression
Percent Expressed
D.
% of total cells (myeloid)
granulocytic
macrophages
APCs
monocytes
microglia
RVFV
WT
Mavs-/-
E.
RVFV
Mavs-/-
WT
Ifna2 Ifnb1
Average Expression
Percent Expressed
F.
response to virus (GO:0009615)
neg. reg. of viral genome replication (GO:0045071)
antigen processing and presentation (GO:0019882)
response to type I interferon (GO:0034340)
-log10(FDR)
G.
response to il-1 (GO:0070555)
regulation of chemokine production (GO:0032642)
positive regulation of cell adhesion (GO:0045785)
positive regulation of il-6 production (GO:0032755)
-log10(FDR)
H.
Expression levels
Irf7 Isg15 Isg20 Oasl1
Ifit1 Ifit3 Ifi27l2a Bst2
Irf1 Irf8 Il1b Nos2
WT– WT+ Mavs-/- – Mavs-/- +
I.
RVFV+ MG (%)
***
WT Mavs-/-
J.
MFI (CD86)
****
****
ns
***
ns
ns
ns
WT Mavs-/-
K.
MFI (I-A/I-E)
***
ns
ns
**
***
****
ns
WT Mavs-/-
uninf
uninf (w/inf)
inf

Fig 6. Microglia from *Mavs*$^{-/-}$ brains have defective response to RVFV infection. UMAP plots depicting cell clusters of myeloid lineage cells derived from WT and *Mavs*$^{-/-}$ brains, +/- RVFV infection. Cell types (A) or conditions (B) are color coded. Gene markers for specific cell types (C). The distribution of myeloid lineage cell types within brains of each condition (D). Expression of type I IFNs within microglia (clusters 0 and 1) (E). Gene ontology (GO) enrichment analysis showing pathways enriched in WT vs *Mavs*$^{-/-}$, or *Mavs*$^{-/-}$ vs WT microglia (clusters 0 and 1) from infected brains are shown in (F) and (G), respectively. Violin plots depicting the relative expression of selected genes within microglia (clusters 0 and 1) are shown in (H). Flow cytometry: microglia were defined as CD11b^{int} CD45^{int} as described in Fig 5, and the percentage of RVFV^{+} microglia are shown in (I). Mean fluorescence intensities (MFI) of CD86 and I-A/I-E expression on microglia (J) and (K), respectively. Data in (I-K) are shown as the mean +/- SD. $^{**}p<0.01$, $^{***}p<0.001$, $^{****}p<0.0001$.

https://doi.org/10.1371/journal.ppat.1010231.g006

(Fig 7A–7D). Lymphocytes comprised greater than 30% of the total sequenced cells in the *Mavs*$^{-/-}$ infected condition (Figs 5D and 7D and S4B). There was also a larger subset of proliferating lymphocytes in *Mavs*$^{-/-}$ infected brains versus WT (Fig 7D). Upon examining genes that were differentially expressed between WT and *Mavs*$^{-/-}$ lymphocytes, we observed defects in ISG expression (*Irf7*, *Ifi44*, *Xcl1*), as well as genes involved in T and NK cell-mediated killing (*Prf1*, *Gzmb*, *Ifng*) [42] within lymphocytes from *Mavs*$^{-/-}$ infected animals (Fig 7E), suggesting that *Mavs*$^{-/-}$ cells are less efficient in clearing the virus than WT cells [43–45]. A similar pattern of gene expression was also observed within lymphocytes isolated from female infected brains (S4F Fig). Consistent with this, we observed reduced expression of *Il15*, *Il18*, and *Il27*, cytokines that have a stimulatory effect on T and NK cells [46–49], in microglia from infected *Mavs*$^{-/-}$ mice (S6 Fig). Lower levels of IFN-γ protein were also detected in the brains of *Mavs*$^{-/-}$ versus WT infected mice (Fig 7G). Taken together, these results suggest that a defective response of *Mavs*$^{-/-}$ microglia may lead to the reduced capacity of T and NK cells to control RVFV infection.

Discussion

Despite the major role of pathogenesis in the brain for the most severe outcomes of RVFV infection, there has been little investigation of local antiviral immune responses within this organ. Here, we investigated the innate immune response in the brain to RVFV in a mouse model of intranasal infection. We demonstrated that microglia mount a robust response to RVFV that is dependent on MAVS and independent of TLR3 and TLR7. To probe viral pathogenesis in the brain in the presence and absence of a functional innate immune response, we profiled the brains of WT and *Mavs*$^{-/-}$ animals following intranasal infection with RVFV. *Mavs*$^{-/-}$ animals succumbed to infection more rapidly with significantly higher viral titers in the brain. Viral presence in the brain corresponded with massive immune infiltration in both WT and *Mavs*$^{-/-}$ mice, consisting mostly of myeloid lineage cells as well as some lymphocytes, with significantly more T and NK cells in the brains of *Mavs*$^{-/-}$ animals. Robust immune gene expression was observed in the brains of both WT and *Mavs*$^{-/-}$ infected animals, with greater inflammatory gene expression within *Mavs*$^{-/-}$ brains. Deficiencies in type I IFN expression were noted within whole brain tissue as well as specifically within microglia in *Mavs*$^{-/-}$ infected animals. Furthermore, microglia from *Mavs*$^{-/-}$ animals displayed deficiencies in downstream antiviral signaling pathways and ISG expression. T and NK cells from *Mavs*$^{-/-}$ animals were also deficient in ISG expression, genes related to killing functions, and *Ifng* expression resulting in lower levels of IFN-γ protein.

Previous studies using mouse models of infection suggest that failure to establish a robust peripheral immune response to RVFV infection allows for viral spread to the brain, and exposure via the respiratory route increases the likelihood of bypassing such a protective response [4,5,26,27,50]. Thus, the primary function of a protective response is to prevent the virus from reaching the brain; however, a recent study using a rat model of infection provided additional insight into the role of immune responses within the brain. Albe *et. al* [7] observed that rats infected subcutaneously with RVFV had detectable viral RNA in the brain as early as one day

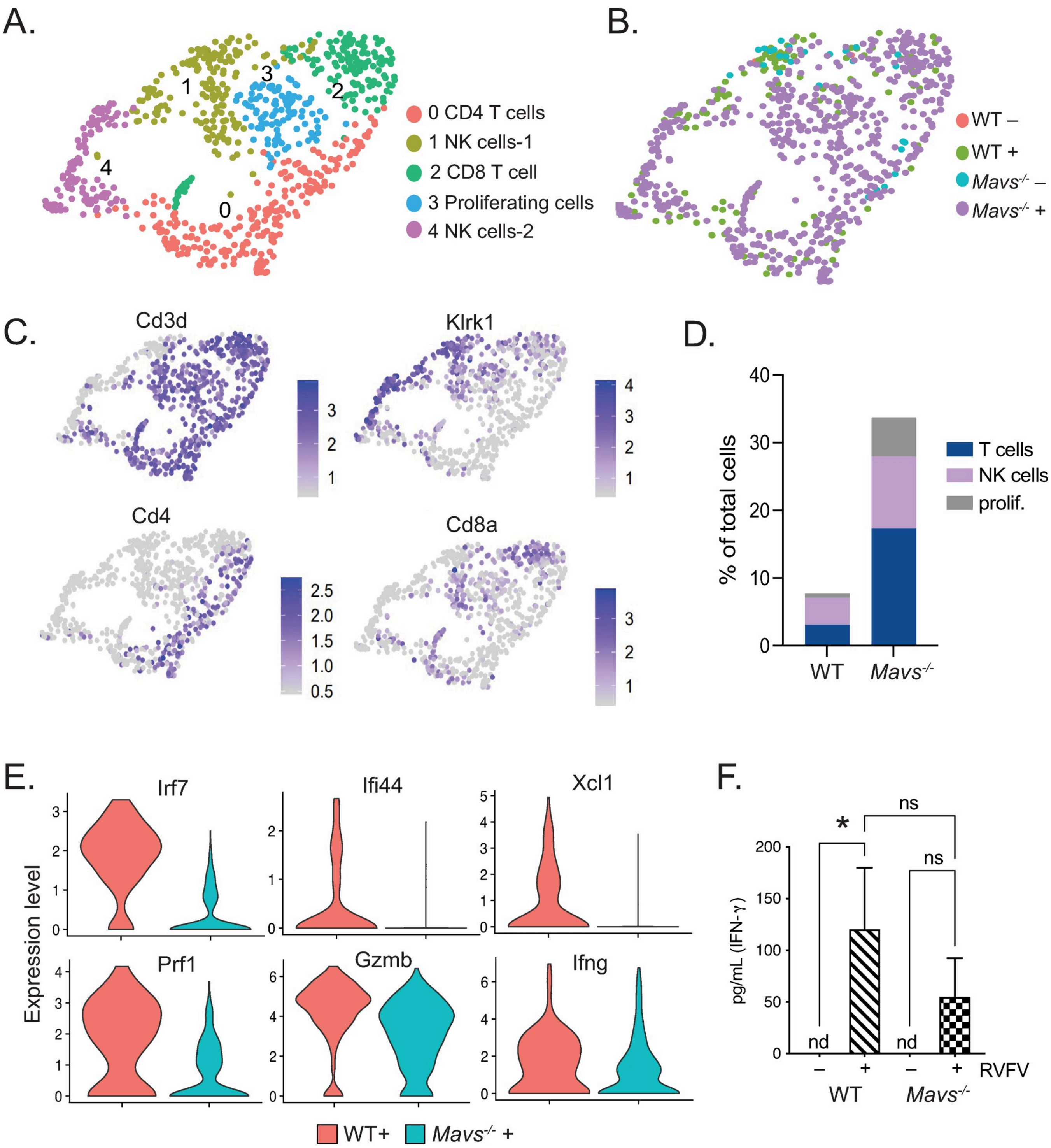

Fig 7. Dysregulated pattern of lymphocyte infiltration and gene expression in brains of *Mavs*$^{-/-}$ mice. UMAP plots depicting cell clusters of lymphoid lineage cells derived from WT and *Mavs*$^{-/-}$ brains, +/- RVFV infection. Cell types (A) or conditions (B) are color coded. Feature plots showing expression of cell type specific markers are shown in (C). The distribution of lymphoid lineage cell types within brains of infected mice (D). Violin plots depicting the relative expression of selected genes within all lymphocytes are shown in (E). Quantitation of IFN-γ is depicted in (F). $^{*}p<0.05$.

https://doi.org/10.1371/journal.ppat.1010231.g007

post-infection despite lacking overt signs of disease. Furthermore, T cell infiltration into the brain was associated with survival, suggesting that functional T cell responses are capable of clearing infection and promoting recovery. Rats exposed to aerosolized RVFV did not display T cell infiltration in the brain and ultimately succumbed to infection. This study is consistent with the hypothesis that the lack of a robust peripheral immune response leads to increased pathogenesis within the brain, however it suggests that extension of peripheral responses to the brain is critical for the resolution of RVFV infection. Work presented in this study support the critical role of innate immune responses to RVFV within the brain and additional characterization of the recruitment and orchestration of this protective response warrants further investigation.

Evaluation of RVFV pathogenesis in the brain has been complicated by variance in disease manifestation depending on virus strain, animal model, and route of infection. Moreover, the requirement for high containment of fully virulent strains can limit the types of analyses performed. Here, we demonstrate that a subset of WT C57BL/6 mice infected intranasally with RVFV MP-12 develop neuroinvasive disease, evidenced by recovery of live virus, inflammatory gene expression, and immune cell infiltration within the brain. In addition, our study includes comparison of gene expression changes within microglia infected with MP-12 and ZH501. Microglia have a less robust response to ZH501 relative to MP-12, although still induced significant expression of various immune genes including *Ifnb1*, *Ifna2*, *Cxcl10*, and *Il6*, among others. This is consistent with prior reports that WT RVFV induces a more attenuated immune response [32], which contributes to its virulence. Future work is necessary to compare our *in vivo* results obtained with MP-12 to an infection model that utilizes fully virulent RVFV. Previous work comparing gene expression *in vitro* within rodent microglia of different ages demonstrated that microglia acquired a more reactive phenotype over time, with higher levels of "sensome" and inflammatory genes [51–53]. This could suggest that microglia in the brains of adult mice may be more primed to react to viral infection *in vivo* than the neonatal microglia used for *in vitro* studies and furthermore, microglia *in vivo* may respond more robustly to ZH501 infection than is suggested by our *in vitro* data.

Our results indicate that RVFV readily infects microglia, which then primarily utilize the RLR pathway *via* the signaling adaptor MAVS to detect and respond to RVFV infection, with microglia derived from *Mavs*$^{-/-}$ animals displaying diminished type I IFN and IFN-responsive gene expression and reduced capacity to upregulate surface markers of activation or secrete cytokines. While we did not determine the role of RLR sensors RIG-I and MDA5 in the recognition of RVFV by microglia upstream of MAVS, previous work has indicated a role for both receptors in the response of DCs to RVFV [6], with RIG-I playing a greater role than MDA5. Further work is needed to define which of these receptors are most critical in the response to RVFV by microglia. *In vitro*, microglia derived from *Mavs*$^{-/-}$ animals displayed abrogated antiviral responses including diminished type I IFN and IFN-responsive gene expression and diminished capacity to upregulate surface markers of activation or secrete cytokines. Our *in vitro* data suggest that TLR3 and 7 play little to no role in the response of microglia to RVFV infection; however, we cannot rule out a role for these receptors in the response of other cells of the brain. Interestingly, while only 2 genes demonstrated significantly different expression between WT and *Tlr3*$^{-/-}$ microglia, 9 genes were significantly different between WT and *Tlr7*$^{-/-}$ microglia, with both *Ifnb1* and *Ifna2* expression significantly decreased in *Tlr7*$^{-/-}$ cells. Moreover, a small amount of *Ifnb1* induction (2.6-fold) was observed within *Mavs*$^{-/-}$ microglia. Although speculative, these data may suggest that while MAVS clearly plays a dominant role in the response of microglia to RVFV infection, TLR7 may also be involved. Further *in vivo* studies are necessary to define any role for TLR7 or TLR3 in RVFV pathogenesis of the brain.

The centrality of MAVS in the response of microglia to RVFV *in vitro* is clear, with equivalent levels of viral infection inducing an extremely attenuated response in MAVS-deficient cells. The assessment of the *in vivo* response is complicated by the differences in viral burden, with higher levels of viral antigen in *Mavs*$^{-/-}$ animals undoubtedly contributing to greater inflammatory signaling and cellular infiltration. scRNA-seq analysis provides increased resolution on the *in vivo* response, enabling assessment of MAVS-specific defects in type I IFN production by microglia, astrocytes, and oligodendrocytes, and in IFN-responsive gene expression by microglia/myeloid cells that was not evident in the bulk RNA sequencing analysis. Pathways that were enriched in WT microglia versus *Mavs*$^{-/-}$ included response to virus and negative regulation of viral genome replication, indicating that WT microglia have a greater capacity to control viral infection. Specific ISGs with demonstrated antiviral activity were elevated including *Ifit1* and *Ifit3*, both of which have previously been shown to bind RVFV genomic RNA and have inhibitory activity on viral growth [54]. Further investigation is required to determine if these ISGs have anti-RVFV activity in microglia. Other ISGs that were among the 20 most upregulated genes in WT microglia include master regulatory genes *Irf7* and *Isg15*, broad spectrum exonucluease *Isg20*, *Ifi27l2a*, which has been shown to have antiviral activity against WNV [55], and *Oasl1*, which can regulate *Irf7* expression [56].

Using flow cytometry, we demonstrated that WT microglia upregulate CD86 and I-A/I-E on the cell surface in response to RVFV infection. Upregulation of surface markers was restricted to microglia that were RVFV^{+}, which were of relatively low abundance in WT brains. Separating microglia from infected brains into RVFV^{+} and RVFV^{-} populations was restricted to antibody staining and was not possible using scRNA-seq due to the sequencing technology being unable to capture RVFV genomic RNA. While we cannot ascertain which sequenced microglia were infected or uninfected, it can be inferred that the changes in gene expression observed within WT microglia were induced largely in trans in response to secreted factors from neighboring cells due to the low levels of infection detected by antibody staining. Adaptation of the sequencing technology to allow capture of the RVFV genome would provide further resolution on the issue of differential cellular tropism within the brain, which has not been thoroughly investigated for RVFV. Previous work has provided ultrastructural evidence for infection of neurons, as well as “neuroglial” cells, based on morphology [50,57]. Notably, neurons were found to harbor large numbers of viral particles. Our work indicated that the primary producers of type I IFN were astrocytes, oligodendrocytes, and microglia. Further work is necessary to characterize whether direct infection of these cell types is necessary for IFN induction, and also to investigate a role for the subversion of IFN responses specifically within neurons in RVFV-infected brains.

Microglia from *Mavs*$^{-/-}$ brains displayed much higher levels of infection, ranging from 15–50% of the total microglia. *Mavs*$^{-/-}$ microglia upregulated genes enriched in inflammatory processes such as response to interleukin-1 and positive regulation of interleukin-6. *Mavs*$^{-/-}$ microglia upregulated surface expression of I-A/I-E, on both RVFV^{+} and RVFV^{-} microglia *in vivo*. Antigen processing and presentation was observed transcriptionally only within WT microglia, therefore the functional significance of I-A/I-E expression is unclear. Interestingly, *Irf1*, *Irf8*, and *Il1b* were amongst the genes most upregulated in *Mavs*$^{-/-}$ microglia versus WT. Previous studies utilizing a mouse model of nerve injury indicated increased *Il1b* expression by microglia that was dependent on *Irf1* and *Irf8* expression [39,40]. These studies in conjunction with our present study suggest that different types of pathological insults can activate a common inflammatory state in microglia and failure to establish an appropriate antiviral response may dispose the microglia to remain in a proinflammatory state.

The lack of MAVS also resulted in dysregulated cellular infiltration into the brain. Myeloid and lymphoid lineage cells are recruited into the brains of both WT and *Mavs*$^{-/-}$ infected mice, and while the numbers and subtype distribution of infiltrating myeloid cells are similar, the lymphocytes very greatly between the two genotypes. Brain infiltrating lymphocytes consisted of T and NK cells in both WT and *Mavs*$^{-/-}$ animals however more NK than T cells were observed in WT. The impact of either cell type, both in terms of controlling infection or exacerbating disease, is unclear. Furthermore, the T and NK cells in the brains of *Mavs*$^{-/-}$ mice appear to be functionally deficient due to decreased expression of ISGs and genes related to killing functions. The role of NK cells in controlling RVFV infection has not been investigated, and our data indicating elevated expression of ISGs and genes related to killing functions suggest they may play an active role in controlling infection within the brain. Excessive numbers of T cells are likely recruited to the brains of *Mavs*$^{-/-}$ mice due to the increased presence of viral antigen, but may be functionally deficient and therefore less able to control viral replication. This is in line with previous studies investigating the role of MAVS in WNV infection which demonstrated increased infiltration of T cells with lower functional avidity into the brains of *Mavs*$^{-/-}$ mice [30,58]. Moreover, their presence may be contributing to the overall inflammatory environment in the brains of *Mavs*$^{-/-}$ mice and thus exacerbating disease [59]. Interestingly, we observed increased expression of *Il15*, *Il18*, and *Il27*, which have been shown to activate T and NK cells [46–49], in WT microglia and other myeloid cells. Secretion of these cytokines may be one mechanism by which microglia regulate the cytotoxic activity of lymphocytes, and lack of expression in *Mavs*$^{-/-}$ microglia could be playing a role in the defective lymphocyte responses observed in these animals. Future studies will explore the relationship between secreted factors from microglia and the induction of protective T and NK cell responses, as well as the role of infiltrating myeloid cells, during RVFV infection of the brain. Taken together, previous studies and our present study indicate that RLR signaling through MAVS is required not only to control viral replication early but is also necessary to induce a fully functional adaptive response.

In summary, this present work provides a better understanding of the immune response in the brain to RVFV infection. Furthermore, it defines a protective role for MAVS in propagating antiviral responses in the brain and suggest that signaling through MAVS may also be required for functional T and NK cell responses in the brain. Better understanding of the immune responses that are active against RVFV in the brain may contribute to therapeutics that effectively harness or augment these responses and lead to treatments for encephalitic disease.

Materials and methods

Ethics statement

All animal work was approved by the Lawrence Livermore National Laboratory Institutional Animal Care and Use Committee under protocol #256. All animals were housed in an Association for Assessment and Accreditation of Laboratory Animal Care (AAALAC)-accredited facility.

Cells and viruses

Vero, EOC 13.31, SIM A9, and LADMAC cells were obtained from the American Type Culture Collection (ATCC). Cell lines were maintained in the following culture media: Vero: Dulbecco's modified Eagle's medium (DMEM) supplemented with 10% fetal bovine serum (FBS). EOC 13.31: DMEM supplemented with 10% FBS and 20% LADMAC conditioned media to provide a source of CSF-1 to support microglial growth [60]. SIM-A9: DMEM:F12 supplemented with 10% FBS and 5% horse serum. LADMAC: Minimal essential medium supplemented with 10% FBS. Primary glial cells: RPMI 1640 supplemented with 10% FBS and 0.01

mg/mL gentamicin and 0.25 μg/mL amphotericin. All media was supplemented with 100 units/ml penicillin and 100 μg/ml streptomycin, and all cells were maintained at 37˚C in 5% CO2. All cell culture reagents were obtained from Thermo Fisher. LADMAC conditioned media was prepared by collecting supernatant from confluent cells that have been in culture for 5–7 days and centrifuged at 300 x *g* for 10 min to remove cellular debris.

Wild type Rift Valley fever virus (RVFV) strain ZH501 was obtained from the NIH Biodefense and Emerging Infections Research Resources Repository, NIAID, NIH. The MP-12 strain was kindly provided by Oscar Negrete (Sandia National Laboratory). RVFV stocks were propagated in Vero cells as previously described [61,62]. Titers of viral stocks were determined by standard plaque assay consisting of an agarose overlay and crystal violet staining. All work with the ZH501 strain was performed in Institutional Biosafety Committee approved BSL-3 and ABSL-3 facilities at Lawrence Livermore National Laboratory using appropriate PPE and protective measures.

Mice

C57BL/6 as well as mice genetically deficient in MAVS *(*B6;129-*Mavs*^{tm1Zjc}*/J*; Jax stock No: 008634*)*, TLR3 B6;129S1-*Tlr3*^{tm1Flv}/J; Jax Stock No: 005217), and TLR7 (B6.129S1-*Tlr7*^{tm1Flv}/J; Jax stock No: 008380) were obtained from Jackson Laboratory. For experiments using knockout (KO) mice, animals were crossed to WT C57BL/6 mice to generate a heterozygous F1 generation. F1 littermates were crossed to generate homozygous WT and KO F2 progeny. Matched WT and KO animals from the same generation were used for each genotype. All animals were maintained in PHS-assured facilities.

Isolation of primary microglia isolation

Primary microglia were isolated and cultured as described previously [63,64]. Briefly, brains from 1–4-day old neonatal mice were dissected to remove meninges and large blood vessels and finely minced with sterile surgical scissors. The minced tissue was then forced through a 70 μM cell strainer (Fischer Scientific) and rinsed with cold glial media. Cells were pelleted at 300 x *g* for 10 min then resuspended in 20 mL fresh media and placed in a T75 flask (1 flask per 7–9 brains) and maintained in culture for 2 weeks. Microglia were harvested from the mixed glial culture by shaking flasks for 4 h at 200 rpm using an orbital shaker. Cells were pelleted at 300 x *g* for 10 min and resuspended in 10 mL microglia growth media (glial media + 20% LADMAC conditioned media). Microglia from up to 3 T75 flasks were combined and placed in a T25 flask. Microglia were maintained in culture for up to one week before use in viral infection experiments.

In vitro infection of microglia

Microglia were plated in 24 well tissue culture treated plate at a density of 250,000 cells per well in primary glial cell media. Cells were infected with RVFV at a MOI of 5 (qPCR analysis) or 2 (flow cytometry, cytokine analysis, and assessment of viral titer in supernatant) in primary glial cell media. Cells were incubated with virus for 4 h at 37˚C in 5% CO_2. Viral infection media was then removed, and cells used for qPCR analysis were lysed for RNA extraction. Cells used for flow cytometry, cytokine analysis, and assessment of viral titer in supernatant were washed one time with PBS, then replenished with fresh media and incubated for another 18–24 h. Supernatants were then removed and stored at -80˚C for cytokine and titer analysis, and cells were processed for flow cytometric analysis. Data for all *in vitro* assays presented are displayed as the average from triplicate wells and are representative of experiments performed at least twice.

Cytokine analysis

Cytokines were quantified using Legendplex multiplex bead-based assay (Biolegend) using the mouse anti-virus response panel according to manufacturer's instructions. Flow cytometry of the beads was performed using a FACSAria Fusion and data were analyzed using Biolegend's cloud-based analysis software available at https://legendplex.qognit.com.

In vivo infection and brain tissue isolation and preparation

Groups of male and female *Mavs*$^{-/-}$ and wildtype (WT) control littermates ranging in age from 8–12 weeks were inoculated intranasally with $5x10^5$ (MP-12, n = 12) or 1000 PFU (ZH501, n = 20) RVFV while under anesthesia (4–5% isoflurane in 100% oxygen). Mice were monitored daily for signs of morbidity and animals were humanely euthanized upon signs of severe disease by CO_2 asphyxiation. For tissue harvest, animals were euthanized by CO_2 asphyxiation and the whole animal was perfused with 30 mL sterile PBS containing 50,000 U/L sodium heparin *via* the left ventricle.

Brain tissue isolation and preparation

Brains for flow cytometric, RNA sequencing, cytokine, and viral titer analysis were isolated from MP-12 infected mice on day 7 post-infection. A total of 12 mice (infected) or 5 mice (uninfected) per genotype were analyzed in 2 independent experiments. Data for flow cytometry and cytokine analysis on infected animals are shown only for WT mice that had detectable live virus in the brain (n = 5), and for *Mavs*$^{-/-}$ mice that survived to day 7 (n = 11). RNA sequencing was performed on RNA isolated from 3 (WT uninfected, *Mavs*$^{-/-}$ uninfected, *Mavs*$^{-/-}$ infected) or 2 (WT infected) brains per condition.

Preparation of brain tissue was performed as previously described [65]. Following euthanasia and perfusion, brains were removed and placed in digestion buffer (PBS pH 7.4 (Thermo Fisher) + liberase + DNase I (both from Roche) to a final concentration of 1.6 wunsch/mL and 0.5 mg/mL, respectively) on ice in a 1.5 mL tube. Brains were finely diced into 1–2 mm^3 pieces with scissors. 3–4 pieces were placed into RNAlater (Qiagen) for gene expression analysis. The remaining tissue was digested at 37˚C for 30 min. EDTA was added to a final concentration of 10 mM to stop the digestion reaction. A cell suspension was generated by gentle pipetting followed by passage through a 70 μm cell strainer. The cell strainer was rinsed with PBS supplemented with 5% FBS to a total volume of 20 mL. Aliquots of this suspension were stored at -80˚C for cytokine and viral titer analysis. The remaining suspension was subjected to Percoll gradient centrifugation to purify mononuclear immune cells for flow cytometric analysis as previously described [65].

Flow cytometry

Cells were incubated for 30 min on ice in 100 μl Hank's balanced salt solution (Thermo Fisher) + 2% FBS with Fc block (1:100 dilution, clone 2.4G2; BD Biosciences) along with the following antibodies (all from BD Biosciences): CD45 APC-Cy7 (1:500, clone 30-F11), CD11b AF488 (1:500, clone M1/70), CD80 BV421 (1:200, clone 16-1OA1), and CD86 PE-Cy7 (1:500, clone GL1). IA/I-E AF647 (1:500, clone M5/114.15.2; BioLegend). Cells were then fixed and permeabilized using BD Cytofix/Cytoperm (BD Biosciences) according to manufacturer's instructions. Cells were then incubated with an anti-RVFV antibody (kindly provided by Dr. Robert Tesh and the World Reference Center of Emerging Viruses and Arboviruses) at 1:500 dilution, followed by goat anti-mouse PE secondary antibody (1:1000, Santa Cruz biotechnology). Flow cytometry was performed using a FACSAria Fusion and data were analyzed using FlowJo software. Microglia, other myeloid lineage, and lymphocytes were resolved using CD45 and CD11b expression, with microglia identified as $CD45^{int}$ $CD11b^{int}$, other myeloid as $CD45^{hi}$ $CD11b^{hi}$, and lymphocytes as $CD45^{hi}$ $CD11b^{-}$ as previously described [65].

qPCR and bulk RNA seq analyses

RVFV genomic RNA was quantified in *in vitro* cultured microglia and brain tissue as described previously [5,26,66]. To normalize between samples, results were normalized to GAPDH expression. For *in vitro* qPCR analysis of immune gene expression, RNA from infected and uninfected microglia was harvested at 4 h post-infection using RNeasy plus kits, and cDNA was generated using RT^2 First Strand Synthesis kit (both from Qiagen) according to manufacturer's instructions. Real-time quantitative RT-PCR analysis of the samples was carried out using the mouse antiviral response RT^2 Profiler PCR array (Qiagen) on a 7900HT Fast Real-Time PCR system (Thermo Fisher) according to manufacturer's instructions. Data were analyzed using Qiagen's online analysis software available at https://geneglobe.qiagen.com/us/analyze. Data are shown as the $\log_2$ fold change in gene expression in infected versus uninfected samples.

For bulk sequencing analysis, RNA was harvested from RNAlater preserved brain tissue using RNeasy Plus kit. Poly(A)+-enriched cDNA libraries were generated using the Illumina TruSeq RNA Library Prep kit v2 (Illumina Inc). The 75 bp single-end reads were sequenced was performed using an Illumina (Illumina Inc) NextSeq 500 instrument. Sequencing data quality was checked using FastQC software. Reads were mapped to the mouse reference genome (mm10) using STAR [67]. Read counts per gene locus were summarized with featureCounts [68]. Then the data was normalized using RUVseq [69] to correct for batch effects and other unwanted variations. Genes differentially expressed between uninfected and infected samples were identified using edgeR [70]. Gene ontology (GO) and pathway enrichment analysis was performed using functional annotation tool ToppGene [71]. Heatmaps were generated using heatmap.2 function in 'gplots' R package.

Single cell RNA sequencing

Mice were euthanized and perfused as described above. Isolated brain tissues were immediately processed using a modified protocol from [72]. Cortices were dissected in cold Hibernate A medium (BrainBits LLC) and sliced to approximately 0.5 mm before transferred to a 15 mL falcon tube with Hibernate A and B27 medium (HABG) (Thermo Fischer Scientific). Collected tissue samples in 15 mL conical tubes were warmed up to 30˚C in a shaking water bath for 8 minutes, before the HABG supernatant replaced with activated papain (34 U/mL, Worthington Biochemical Corporation) and the tubes placed back into the shaking water bath for tissue digestion (30˚C, 150 rpm) for 30 minutes. Cells were released from the digested tissues by trituration using a fire-polished Pasteur pipette. Released cells were collected in the supernatant and filtered through a 70 mm MACS Smart Strainer (Miltenyi Biotec) into a new 15 mL conical tube. The single cell suspension was layered onto a Optiprep density gradient to separate cells from debris, after centrifugation (800 x *g*, 15 min, 22˚C). The debris fraction was collected, and the gradient material diluted with HAGB before tubes were centrifuged (200 x *g*, 5 min, 22˚C). The supernatant was aspirated, and ACK lysis buffer (Thermo Fisher Scientific) was added to the cell suspension remove any remaining red blood cells (5 min, RT). Hank's balanced salt solution (Thermo Fisher) was added to the cell suspension containing the lysis buffer and tubes were centrifuged (200 x *g*, 5 min, 22˚C). To remove dead cells from the single cell suspension, a Dead cell removal kit (Miltenyi Biotec) was used as directed by the vendor.

Cell pellets were resuspended in PBS with 0.04% non-acetylated BSA and counted on a Countess II automated cell counter prior to single-cell sequencing preparation using Chromium Single-cell 3′ GEM, Library & Gel Bead Kit v3 (10x Genomics Cat # 1000075) on a 10× Genomics Chromium Controller following manufacturers' protocol. Sequencing data was demultiplexed, quality controlled, and analyzed using Cell Ranger (10x Genomics) and Seurat [73]. The Cell Ranger Single-Cell Software Suite was used to perform sample demultiplexing, barcode processing, and single-cell 3′gene counting. Samples were first demultiplexed and then aligned to the mouse genome (mm10) using "cellranger mkfastq" with default parameters. Unique molecular identifier counts were generated using "cellranger count". Further analysis was performed using Seurat [73]. First, cells with fewer than 500 detected genes per cell and genes that were expressed by fewer than 5 cells were filtered out. After pre-processing, we performed data normalization, scaling, and identified 2000 most variable features. Then, anchors for data integration were identified using the 'Find-IntegrationAnchors' function. Next, these anchors were passed to the 'IntegrateData' function and new integrated matrix with all four datasets were generated. Subsequently, dimensionality reduction, clustering, and visualization were performed in Seurat as described before [74]. Genes differentially expressed between clusters were identified using 'FindMarkers' function implemented in Seurat.

Statistical analyses

Data were analyzed and graphed using Prism (GraphPad, La Jolla, CA) software. For qPCR, significance was determined using a 2-way ANOVA test comparing average expression between genotypes or gene expression changes beyond the 95% confidence intervals (CI) of infected and uninfected samples. For flow cytometry and cytokine analyses, significance was assessed using unpaired *t* test, or one or two-way ANOVA with Tukey's multiple comparisons test. Survival data were analyzed for significance using the Log-rank (Mantel-Cox) test. An adjusted p value of 0.05 or less was considered significant, and significant differences are indicated as follows: $^{*}p < 0.05$, $^{**}p < 0.01$, $^{***}p < 0.001$, $^{****}p < 0.0001$.

Supporting information

S1 Fig. Infection of primary microglia is not dependent upon genotype. Primary microglia derived from WT or the indicated genetically deficient mice were infected with RVFV MP-12 and the percentage of cells positive for RVFV was assessed by flow cytometry (A) or levels of RVFV genomic RNA were assessed by qPCR (B). Primary microglia derived from WT or *Mavs*$^{-/-}$ mice were infected with RVFV MP-12, supernatants collected at 24 hours post-infection, and viral titers in supernatants assessed by plaque assay (C).
(TIF)

S2 Fig. Expression of activation markers is not dependent on TLR3 or TLR7. Microglia derived from WT or *Tlr3*$^{-/-}$ (A) or *Tlr7*$^{-/-}$ (B) mice were infected with RVFV MP-12 and at 18–24 hours post-infection, cells were harvested for flow cytometry. The expression levels of the indicated activation markers were assessed on uninfected cells (black bars), uninfected cells in culture with infected cells (uninf (w/ inf), gray bars), and infected cells (inf, white bars) and shown as the mean fluorescence intensity of the indicated activation markers. Data are shown as the mean +/- SD $^{*}p <0.05$, $^{**}p<0.01$, $^{***}p<0.001$, $^{****}p<0.0001$
(TIF)

S3 Fig. RVFV is detected in the brain on day 7 post-infection. WT mice were infected intranasally with $5x10^5$ PFU RVFV MP-12 and brains were harvested on the indicated day post-

infection for viral quantitation.
(TIF)

S4 Fig. Single cell RNA sequencing supplemental information. Gene markers for specific cell types defining the cell clusters in Fig 5A (A). The distribution of cell types within female infected brains (B). Expression of type I IFNs within astrocytes (Fig 5A cluster 1, C) and oligodendrocytes (Fig 5A cluster 7, D). Violin plots depicting the relative expression of selected genes within microglia from female infected brains (E). Dot blot depicting gene expression within lymphocytes from female infected brains (F).
(TIF)

S5 Fig. CD80 expression on microglia. Mean fluorescence intensity of CD80 on microglia isolated from the brains of WT and *Mavs*$^{-/-}$ mice, +/- RVFV infection.
(TIF)

S6 Fig. Microglia and myeloid cells from *Mavs*$^{-/-}$ infected brains display lower levels of cytokine gene expression.
(TIF)

S1 Table. Relative expression of antiviral genes across genotypes and RVFV strains.
(XLSX)

S2 Table. Differential gene expression in whole brain infected vs uninfected.
(XLSX)

Acknowledgments

This work was performed under the auspices of the U.S. Department of Energy by Lawrence Livermore National Security, LLC, Lawrence Livermore National Laboratory under Contract DE-AC52-07NA27344.

Author Contributions

Conceptualization: Nicholas R. Hum, Feliza A. Bourguet, Dina R. Weilhammer.

Data curation: Nicholas R. Hum, Feliza A. Bourguet, Aimy Sebastian, Dina R. Weilhammer.

Funding acquisition: Dina R. Weilhammer.

Investigation: Nicholas R. Hum, Feliza A. Bourguet, Doris Lam, Ashlee M. Phillips, Kristina R. Sanchez, Amy Rasley, Dina R. Weilhammer.

Methodology: Nicholas R. Hum, Feliza A. Bourguet, Aimy Sebastian, Doris Lam, Dina R. Weilhammer.

Project administration: Dina R. Weilhammer.

Resources: Gabriela G. Loots.

Supervision: Dina R. Weilhammer.

Visualization: Nicholas R. Hum, Aimy Sebastian.

Writing – original draft: Nicholas R. Hum, Dina R. Weilhammer.

Writing – review & editing: Nicholas R. Hum, Feliza A. Bourguet, Aimy Sebastian, Doris Lam, Amy Rasley, Gabriela G. Loots, Dina R. Weilhammer.

References

1. Pepin M, Bouloy M, Bird BH, Kemp A, Paweska J. Rift Valley fever virus(Bunyaviridae: Phlebovirus): an update on pathogenesis, molecular epidemiology, vectors, diagnostics and prevention. Vet Res. 2010; 41(6):61. https://doi.org/10.1051/vetres/2010033 PMID: 21188836; PubMed Central PMCID: PMC2896810.
2. Rolin AI, Berrang-Ford L, Kulkarni MA. The risk of Rift Valley fever virus introduction and establishment in the United States and European Union. Emerg Microbes Infect. 2013; 2:e81. https://doi.org/10.1038/emi.2013.81 PMID: 26038446
3. Possession, Use, and Transfer of Select Agents and Toxins; Biennial Review of the List of Select Agents and Toxins and Enhanced Biosafety Requirements. Final rule. Fed Regist. 2017; 82(12):6278–94. PMID: 28106357.
4. Reed C, Lin K, Wilhelmsen C, Friedrich B, Nalca A, Keeney A, et al. Aerosol Exposure to Rift Valley Fever Virus Causes Earlier and More Severe Neuropathology in the Murine Model, which Has Important Implications for Therapeutic Development. PLOS Neglected Tropical Diseases. 2013; 7(4):e2156. https://doi.org/10.1371/journal.pntd.0002156 PMID: 23593523
5. Dodd KA, McElroy AK, Jones TL, Zaki SR, Nichol ST, Spiropoulou CF. Rift valley Fever virus encephalitis is associated with an ineffective systemic immune response and activated T cell infiltration into the CNS in an immunocompetent mouse model. PLoS Negl Trop Dis. 2014; 8(6):e2874. Epub 2014/06/13. https://doi.org/10.1371/journal.pntd.0002874 PMID: 24922480; PubMed Central PMCID: PMC4055548.
6. Ermler ME, Yerukhim E, Schriewer J, Schattgen S, Traylor Z, Wespiser AR, et al. RNA Helicase Signaling Is Critical for Type I Interferon Production and Protection against Rift Valley Fever Virus during Mucosal Challenge. Journal of Virology. 2013; 87(9):4846–60. https://doi.org/10.1128/JVI.01997-12 PMID: 23408632
7. Albe JR, Boyles DA, Walters AW, Kujawa MR, McMillen CM, Reed DS, et al. Neutrophil and macrophage influx into the central nervous system are inflammatory components of lethal Rift Valley fever encephalitis in rats. PLoS Pathog. 2019; 15(6):e1007833. Epub 2019/06/21. https://doi.org/10.1371/journal.ppat.1007833 PMID: 31220182; PubMed Central PMCID: PMC6605717.
8. Anyangu AS, Gould LH, Sharif SK, Nguku PM, Omolo JO, Mutonga D, et al. Risk Factors for Severe Rift Valley Fever Infection in Kenya, 2007. The American Journal of Tropical Medicine and Hygiene. 2010; 83(2 Suppl):14–21. https://doi.org/10.4269/ajtmh.2010.09–0293
9. LaBeaud AD, Pfeil S, Muiruri S, Dahir S, Sutherland LJ, Traylor Z, et al. Factors Associated with Severe Human Rift Valley Fever in Sangailu, Garissa County, Kenya. PLoS Negl Trop Dis. 2015; 9(3): e0003548. https://doi.org/10.1371/journal.pntd.0003548 PMID: 25764399
10. Madani TA, Al-Mazrou YY, Al-Jeffri MH, Mishkhas AA, Al-Rabeah AM, Turkistani AM, et al. Rift Valley fever epidemic in Saudi Arabia: epidemiological, clinical, and laboratory characteristics. Clin Infect Dis. 2003; 37(8):1084–92. Epub 2003/10/03. https://doi.org/10.1086/378747 PMID: 14523773.
11. Javelle E, Lesueur A, Pommier de Santi V, de Laval F, Lefebvre T, Holweck G, et al. The challenging management of Rift Valley Fever in humans: literature review of the clinical disease and algorithm proposal. Ann Clin Microbiol Antimicrob. 2020; 19(1):4–. https://doi.org/10.1186/s12941-020-0346-5 PMID: 31969141.
12. Rustenhoven J. A privileged brain. Science. 2021; 374(6567):548. Epub 20211028. https://doi.org/10.1126/science.abl7122 PMID: 34709902.
13. Lampron A, Elali A, Rivest S. Innate immunity in the CNS: redefining the relationship between the CNS and Its environment. Neuron. 2013; 78(2):214–32. Epub 2013/04/30. https://doi.org/10.1016/j.neuron.2013.04.005 PMID: 23622060.
14. Carty M, Reinert L, Paludan SR, Bowie AG. Innate antiviral signalling in the central nervous system. Trends Immunol. 2014; 35(2):79–87. Epub 20131206. https://doi.org/10.1016/j.it.2013.10.012 PMID: 24316012.
15. Singh H, Koury J, Kaul M. Innate Immune Sensing of Viruses and Its Consequences for the Central Nervous System. Viruses. 2021; 13(2). Epub 2021/01/28. https://doi.org/10.3390/v13020170 PMID: 33498715; PubMed Central PMCID: PMC7912342.
16. Denizot M, Neal JW, Gasque P. Encephalitis due to emerging viruses: CNS innate immunity and potential therapeutic targets. The Journal of infection. 2012; 65(1):1–16. Epub 2012/04/10. https://doi.org/10.1016/j.jinf.2012.03.019 PMID: 22484271.
17. Drokhlyansky E, Göz Aytürk D, Soh TK, Chrenek R, O'Loughlin E, Madore C, et al. The brain parenchyma has a type I interferon response that can limit virus spread. Proc Natl Acad Sci U S A. 2017; 114 (1):E95–e104. Epub 2016/12/17. https://doi.org/10.1073/pnas.1618157114 PMID: 27980033; PubMed Central PMCID: PMC5224383.

18. Moseman EA, Blanchard AC, Nayak D, McGavern DB. T cell engagement of cross-presenting microglia protects the brain from a nasal virus infection. Sci Immunol. 2020; 5(48). Epub 2020/06/07. https://doi.org/10.1126/sciimmunol.abb1817 PMID: 32503876; PubMed Central PMCID: PMC7416530.

19. Sanchez JMS, DePaula-Silva AB, Doty DJ, Hanak TJ, Truong A, Libbey JE, et al. The CSF1R-Microglia Axis Has Protective Host-Specific Roles During Neurotropic Picornavirus Infection. Frontiers in Immunology. 2021; 12(3568). https://doi.org/10.3389/fimmu.2021.621090 PMID: 34566948

20. Funk KE, Klein RS. CSF1R antagonism limits local restimulation of antiviral CD8+ T cells during viral encephalitis. Journal of neuroinflammation. 2019; 16(1):22. https://doi.org/10.1186/s12974-019-1397-4 PMID: 30704498

21. Mangale V, Syage AR, Ekiz HA, Skinner DD, Cheng Y, Stone CL, et al. Microglia influence host defense, disease, and repair following murine coronavirus infection of the central nervous system. Glia. 2020; 68(11):2345–60. Epub 20200525. https://doi.org/10.1002/glia.23844 PMID: 32449994; PubMed Central PMCID: PMC7280614.

22. Chhatbar C, Detje CN, Grabski E, Borst K, Spanier J, Ghita L, et al. Type I Interferon Receptor Signaling of Neurons and Astrocytes Regulates Microglia Activation during Viral Encephalitis. Cell Rep. 2018; 25 (1):118–29.e4. Epub 2018/10/04. https://doi.org/10.1016/j.celrep.2018.09.003 PMID: 30282022; PubMed Central PMCID: PMC7103936.

23. Tsai TT, Chen CL, Lin YS, Chang CP, Tsai CC, Cheng YL, et al. Microglia retard dengue virus-induced acute viral encephalitis. Sci Rep. 2016; 6:27670. Epub 20160609. https://doi.org/10.1038/srep27670 PMID: 27279150; PubMed Central PMCID: PMC4899773.

24. Tansey MG, Goldberg MS. Neuroinflammation in Parkinson's disease: its role in neuronal death and implications for therapeutic intervention. Neurobiol Dis. 2010; 37(3):510–8. Epub 20091110. https://doi.org/10.1016/j.nbd.2009.11.004 PMID: 19913097; PubMed Central PMCID: PMC2823829.

25. Zhang G, Wang Z, Hu H, Zhao M, Sun L. Microglia in Alzheimer's Disease: A Target for Therapeutic Intervention. Front Cell Neurosci. 2021; 15:749587. Epub 20211124. https://doi.org/10.3389/fncel.2021.749587 PMID: 34899188; PubMed Central PMCID: PMC8651709.

26. Dodd KA, McElroy AK, Jones ME, Nichol ST, Spiropoulou CF. Rift Valley fever virus clearance and protection from neurologic disease are dependent on CD4+ T cell and virus-specific antibody responses. J Virol. 2013; 87(11):6161–71. Epub 20130327. https://doi.org/10.1128/JVI.00337-13 PMID: 23536675; PubMed Central PMCID: PMC3648110.

27. Harmon JR, Spengler JR, Coleman-McCray JD, Nichol ST, Spiropoulou CF, McElroy AK. CD4 T Cells, CD8 T Cells, and Monocytes Coordinate To Prevent Rift Valley Fever Virus Encephalitis. J Virol. 2018; 92(24). Epub 20181127. https://doi.org/10.1128/jvi.01270-18 PMID: 30258000; PubMed Central PMCID: PMC6258944.

28. Daffis S, Samuel MA, Suthar MS, Gale M Jr., Diamond MS. Toll-like receptor 3 has a protective role against West Nile virus infection. J Virol. 2008; 82(21):10349–58. Epub 2008/08/22. https://doi.org/10.1128/JVI.00935-08 PMID: 18715906; PubMed Central PMCID: PMC2573187.

29. Town T, Bai F, Wang T, Kaplan AT, Qian F, Montgomery RR, et al. Toll-like receptor 7 mitigates lethal West Nile encephalitis via interleukin 23-dependent immune cell infiltration and homing. Immunity. 2009; 30(2):242–53. Epub 2009/02/10. https://doi.org/10.1016/j.immuni.2008.11.012 PMID: 19200759; PubMed Central PMCID: PMC2707901.

30. Suthar MS, Ma DY, Thomas S, Lund JM, Zhang N, Daffis S, et al. IPS-1 is essential for the control of West Nile virus infection and immunity. PLoS Pathog. 2010; 6(2):e1000757. Epub 2010/02/09. https://doi.org/10.1371/journal.ppat.1000757 PMID: 20140199; PubMed Central PMCID: PMC2816698.

31. Hise AG, Traylor Z, Hall NB, Sutherland LJ, Dahir S, Ermler ME, et al. Association of Symptoms and Severity of Rift Valley Fever with Genetic Polymorphisms in Human Innate Immune Pathways. PLoS Negl Trop Dis. 2015; 9(3):e0003584. https://doi.org/10.1371/journal.pntd.0003584 PMID: 25756647

32. Roberts KK, Hill TE, Davis MN, Holbrook MR, Freiberg AN. Cytokine response in mouse bone marrow derived macrophages after infection with pathogenic and non-pathogenic Rift Valley fever virus. J Gen Virol. 2015; 96(Pt 7):1651–63. Epub 2015/03/12. https://doi.org/10.1099/vir.0.000119 PMID: 25759029; PubMed Central PMCID: PMC4635452.

33. Artegiani B, Lyubimova A, Muraro M, van Es JH, van Oudenaarden A, Clevers H. A Single-Cell RNA Sequencing Study Reveals Cellular and Molecular Dynamics of the Hippocampal Neurogenic Niche. Cell Rep. 2017; 21(11):3271–84. https://doi.org/10.1016/j.celrep.2017.11.050 PMID: 29241552.

34. Cougnoux A, Yerger JC, Fellmeth M, Serra-Vinardell J, Martin K, Navid F, et al. Single Cell Transcriptome Analysis of Niemann-Pick Disease, Type C1 Cerebella. Int J Mol Sci. 2020; 21(15). Epub 20200728. https://doi.org/10.3390/ijms21155368 PMID: 32731618; PubMed Central PMCID: PMC7432835.

35. Vanlandewijck M, He L, Mäe MA, Andrae J, Ando K, Del Gaudio F, et al. A molecular atlas of cell types and zonation in the brain vasculature. Nature. 2018; 554(7693):475–80. Epub 20180214. https://doi.org/10.1038/nature25739 PMID: 29443965.

36. Hammond TR, Dufort C, Dissing-Olesen L, Giera S, Young A, Wysoker A, et al. Single-Cell RNA Sequencing of Microglia throughout the Mouse Lifespan and in the Injured Brain Reveals Complex Cell-State Changes. Immunity. 2019; 50(1):253–71.e6. Epub 20181121. https://doi.org/10.1016/j.immuni.2018.11.004 PMID: 30471926; PubMed Central PMCID: PMC6655561.

37. Morimoto K, Nakajima K. Role of the Immune System in the Development of the Central Nervous System. Frontiers in Neuroscience. 2019; 13(916). https://doi.org/10.3389/fnins.2019.00916 PMID: 31551681

38. Goldmann T, Wieghofer P, Jordão MJ, Prutek F, Hagemeyer N, Frenzel K, et al. Origin, fate and dynamics of macrophages at central nervous system interfaces. Nat Immunol. 2016; 17(7):797–805. Epub 2016/05/03. https://doi.org/10.1038/ni.3423 PMID: 27135602; PubMed Central PMCID: PMC4968048.

39. Masuda T, Tsuda M, Yoshinaga R, Tozaki-Saitoh H, Ozato K, Tamura T, et al. IRF8 is a critical transcription factor for transforming microglia into a reactive phenotype. Cell Rep. 2012; 1(4):334–40. Epub 2012/07/27. https://doi.org/10.1016/j.celrep.2012.02.014 PMID: 22832225; PubMed Central PMCID: PMC4158926.

40. Masuda T, Iwamoto S, Mikuriya S, Tozaki-Saitoh H, Tamura T, Tsuda M, et al. Transcription factor IRF1 is responsible for IRF8-mediated IL-1β expression in reactive microglia. J Pharmacol Sci. 2015; 128(4):216–20. Epub 2015/09/01. https://doi.org/10.1016/j.jphs.2015.08.002 PMID: 26318672.

41. Wierońska JM, Cieślik P, Kalinowski L. Nitric Oxide-Dependent Pathways as Critical Factors in the Consequences and Recovery after Brain Ischemic Hypoxia. Biomolecules. 2021; 11(8). Epub 20210726. https://doi.org/10.3390/biom11081097 PMID: 34439764; PubMed Central PMCID: PMC8392725.

42. Voskoboinik I, Whisstock JC, Trapani JA. Perforin and granzymes: function, dysfunction and human pathology. Nature reviews Immunology. 2015; 15(6):388–400. https://doi.org/10.1038/nri3839 PMID: 25998963.

43. Shrestha B, Samuel MA, Diamond MS. CD8+ T cells require perforin to clear West Nile virus from infected neurons. J Virol. 2006; 80(1):119–29. https://doi.org/10.1128/JVI.80.1.119-129.2006 PMID: 16352536; PubMed Central PMCID: PMC1317548.

44. Shi F-D, Ransohoff RM. Nature killer cells in the central nervous system. Natural Killer Cells. 2010:373–83. Epub 2010/01/29. https://doi.org/10.1016/B978-0-12-370454-2.00028–4 PMC7150147.

45. Yao Y, Strauss-Albee DM, Zhou JQ, Malawista A, Garcia MN, Murray KO, et al. The natural killer cell response to West Nile virus in young and old individuals with or without a prior history of infection. PLOS ONE. 2017; 12(2):e0172625. https://doi.org/10.1371/journal.pone.0172625 PMID: 28235099

46. Choi YH, Lim EJ, Kim SW, Moon YW, Park KS, An HJ. IL-27 enhances IL-15/IL-18-mediated activation of human natural killer cells. J Immunother Cancer. 2019; 7(1):168. Epub 20190705. https://doi.org/10.1186/s40425-019-0652-7 PMID: 31277710; PubMed Central PMCID: PMC6612093.

47. Ochayon DE, Waggoner SN. The Effect of Unconventional Cytokine Combinations on NK-Cell Responses to Viral Infection. Frontiers in Immunology. 2021; 12(775). https://doi.org/10.3389/fimmu.2021.645850 PMID: 33815404

48. Nakanishi K. Unique Action of Interleukin-18 on T Cells and Other Immune Cells. Frontiers in Immunology. 2018; 9(763). https://doi.org/10.3389/fimmu.2018.00763 PMID: 29731751

49. Ziblat A, Domaica CI, Spallanzani RG, Iraolagoitia XL, Rossi LE, Avila DE, et al. IL-27 stimulates human NK-cell effector functions and primes NK cells for IL-18 responsiveness. European journal of immunology. 2015; 45(1):192–202. Epub 20141202. https://doi.org/10.1002/eji.201444699 PMID: 25308526.

50. Smith DR, Steele KE, Shamblin J, Honko A, Johnson J, Reed C, et al. The pathogenesis of Rift Valley fever virus in the mouse model. Virology. 2010; 407(2):256–67. Epub 20100917. https://doi.org/10.1016/j.virol.2010.08.016 PMID: 20850165.

51. Thion MS, Low D, Silvin A, Chen J, Grisel P, Schulte-Schrepping J, et al. Microbiome Influences Prenatal and Adult Microglia in a Sex-Specific Manner. Cell. 2018; 172(3):500–16.e16. Epub 20171221. https://doi.org/10.1016/j.cell.2017.11.042 PMID: 29275859; PubMed Central PMCID: PMC5786503.

52. Lively S, Wong R, Lam D, Schlichter LC. Sex- and Development-Dependent Responses of Rat Microglia to Pro- and Anti-inflammatory Stimulation. Frontiers in cellular neuroscience. 2018; 12:433–. https://doi.org/10.3389/fncel.2018.00433 PMID: 30524242.

53. Hanamsagar R, Alter MD, Block CS, Sullivan H, Bolton JL, Bilbo SD. Generation of a microglial developmental index in mice and in humans reveals a sex difference in maturation and immune reactivity. Glia. 2017; 65(9):1504–20. Epub 20170615. https://doi.org/10.1002/glia.23176 PMID: 28618077; PubMed Central PMCID: PMC5540146.

54. Pichlmair A, Lassnig C, Eberle CA, Górna MW, Baumann CL, Burkard TR, et al. IFIT1 is an antiviral protein that recognizes 5'-triphosphate RNA. Nat Immunol. 2011; 12(7):624–30. Epub 2011/06/07. https://doi.org/10.1038/ni.2048 PMID: 21642987.

55. Lucas TM, Richner JM, Diamond MS, Perlman S. The Interferon-Stimulated Gene Ifi27l2a Restricts West Nile Virus Infection and Pathogenesis in a Cell-Type- and Region-Specific Manner. Journal of Virology. 2016; 90(5):2600–15. https://doi.org/10.1128/JVI.02463-15 PMID: 26699642

56. Lee MS, Kim B, Oh GT, Kim Y-J. OASL1 inhibits translation of the type I interferon–regulating transcription factor IRF7. Nature Immunology. 2013; 14(4):346–55. https://doi.org/10.1038/ni.2535 PMID: 23416614

57. Reed C, Steele KE, Honko A, Shamblin J, Hensley LE, Smith DR. Ultrastructural study of Rift Valley fever virus in the mouse model. Virology. 2012; 431(1–2):58–70. Epub 20120609. https://doi.org/10.1016/j.virol.2012.05.012 PMID: 22687428.

58. Zhao J, Vijay R, Zhao J, Gale M Jr., Diamond MS, Perlman S. MAVS Expressed by Hematopoietic Cells Is Critical for Control of West Nile Virus Infection and Pathogenesis. J Virol. 2016; 90(16):7098–108. Epub 20160727. https://doi.org/10.1128/JVI.00707-16 PMID: 27226371; PubMed Central PMCID: PMC4984631.

59. Ai S, Klein RS. Update on T cells in the virally infected brain: friends and foes. Curr Opin Neurol. 2020; 33(3):405–12. https://doi.org/10.1097/WCO.0000000000000825 PMID: 32304440.

60. O'Keefe GM, Nguyen VT, Ping Tang L, Benveniste EN. IFN-γ Regulation of Class II Transactivator Promoter IV in Macrophages and Microglia: Involvement of the Suppressors of Cytokine Signaling-1 Protein. The Journal of Immunology. 2001; 166(4):2260–9. https://doi.org/10.4049/jimmunol.166.4.2260 PMID: 11160280

61. Harmon B, Schudel BR, Maar D, Kozina C, Ikegami T, Tseng CT, et al. Rift Valley fever virus strain MP-12 enters mammalian host cells via caveola-mediated endocytosis. J Virol. 2012; 86(23):12954–70. Epub 20120919. https://doi.org/10.1128/JVI.02242-12 PMID: 22993156; PubMed Central PMCID: PMC3497621.

62. Harmon B, Bird SW, Schudel BR, Hatch AV, Rasley A, Negrete OA. A Genome-Wide RNA Interference Screen Identifies a Role for Wnt/β-Catenin Signaling during Rift Valley Fever Virus Infection. J Virol. 2016; 90(16):7084–97. Epub 20160727. https://doi.org/10.1128/JVI.00543-16 PMID: 27226375; PubMed Central PMCID: PMC4984662.

63. Rasley A, Anguita J, Marriott I. Borrelia burgdorferi induces inflammatory mediator production by murine microglia. Journal of neuroimmunology. 2002; 130(1):22–31. https://doi.org/10.1016/s0165-5728(02)00187-x PMID: 12225885

64. Rasley A, Bost KL, Olson JK, Miller SD, Marriott I. Expression of functional NK-1 receptors in murine microglia. Glia. 2002; 37(3):258–67. https://doi.org/10.1002/glia.10034 PMID: 11857684

65. Martin E, El-Behi M, Fontaine B, Delarasse C. Analysis of Microglia and Monocyte-derived Macrophages from the Central Nervous System by Flow Cytometry. Journal of visualized experiments: JoVE. 2017;(124):55781. https://doi.org/10.3791/55781 PMID: 28671658.

66. Bird BH, Bawiec DA, Ksiazek TG, Shoemaker TR, Nichol ST. Highly sensitive and broadly reactive quantitative reverse transcription-PCR assay for high-throughput detection of Rift Valley fever virus. J Clin Microbiol. 2007; 45(11):3506–13. Epub 2007/09/07. https://doi.org/10.1128/JCM.00936-07 PMID: 17804663; PubMed Central PMCID: PMC2168471.

67. Dobin A, Davis CA, Schlesinger F, Drenkow J, Zaleski C, Jha S, et al. STAR: ultrafast universal RNA-seq aligner. Bioinformatics. 2013; 29(1):15–21. Epub 20121025. https://doi.org/10.1093/bioinformatics/bts635 PMID: 23104886; PubMed Central PMCID: PMC3530905.

68. Liao Y, Smyth GK, Shi W. featureCounts: an efficient general purpose program for assigning sequence reads to genomic features. Bioinformatics. 2014; 30(7):923–30. Epub 20131113. https://doi.org/10.1093/bioinformatics/btt656 PMID: 24227677.

69. Risso D, Ngai J, Speed TP, Dudoit S. Normalization of RNA-seq data using factor analysis of control genes or samples. Nature biotechnology. 2014; 32(9):896–902. Epub 2014/08/24. https://doi.org/10.1038/nbt.2931 PMID: 25150836.

70. Robinson MD, McCarthy DJ, Smyth GK. edgeR: a Bioconductor package for differential expression analysis of digital gene expression data. Bioinformatics (Oxford, England). 2010; 26(1):139–40. Epub 2009/11/11. https://doi.org/10.1093/bioinformatics/btp616 PMID: 19910308.

71. Chen J, Bardes EE, Aronow BJ, Jegga AG. ToppGene Suite for gene list enrichment analysis and candidate gene prioritization. Nucleic Acids Res. 2009; 37(Web Server issue):W305–W11. Epub 2009/05/22. https://doi.org/10.1093/nar/gkp427 PMID: 19465376.

72. Brewer GJ, Torricelli JR. Isolation and culture of adult neurons and neurospheres. Nature Protocols. 2007; 2(6):1490–8. https://doi.org/10.1038/nprot.2007.207 PMID: 17545985

73. Stuart T, Butler A, Hoffman P, Hafemeister C, Papalexi E, Mauck WM, 3rd, et al. Comprehensive Integration of Single-Cell Data. Cell. 2019; 177(7):1888–902.e21. Epub 2019/06/11. https://doi.org/10.1016/j.cell.2019.05.031 PMID: 31178118; PubMed Central PMCID: PMC6687398.

74. Hum NR, Sebastian A, Gilmore SF, He W, Martin KA, Hinckley A, et al. Comparative Molecular Analysis of Cancer Behavior Cultured In Vitro, In Vivo, and Ex Vivo. Cancers (Basel). 2020; 12(3). Epub 20200314. https://doi.org/10.3390/cancers12030690 PMID: 32183351; PubMed Central PMCID: PMC7140030.